Experimental studies of the rheology of a simple liquid mixture during phase separation

A. H. Krall* and J. V. Sengers

Institute for Physical Science and Technology, University of Maryland, College Park, Maryland 20742

K. Hamano

Department of Biological and Chemical Engineering, Faculty of Technology, Gunma University, Kiryu 376, Japan

We report measurements of the effective viscosity and elastic shear modulus of the critical and two off-critical mixtures of isobutyric acid and water in the process of phase separation under shear. All three mixtures exhibit enhancements of the viscosity caused by the presence of concentration domains, as has been suggested by Onuki [Phys. Rev. A **35**, 5149 (1987)]. The critical mixture and an off-critical mixture rich in isobutyric acid also possess significant elasticity during phase separation. Elasticity is absent in the case of a water-rich mixture. During phase separation of the critical mixture, we observe rapid decreases of the viscosity enhancement and the elastic shear modulus. This behavior is due to rapid capillary-driven coarsening of the concentration domains, as we show in a detailed application of a theory recently proposed by Doi and Ohta [J. Chem. Phys. **95**, 1242 (1991)]. The off-critical mixtures exhibit constant viscosity enhancements and, in the case that it is present, an elasticity that increases with time. Some of these features can be understood by regarding the phase-separating off-critical mixtures as dilute emulsions.

I. INTRODUCTION

This paper is devoted to the topic of the stress present in mixtures of simple liquids when they undergo a separating transition under shear. Liquid mixtures undergoing phase separation have been studied extensively ever since it was recognized that, by exploiting the critical slowing down of dynamic processes near the consolute point of two partially miscible liquids, experimenters can make time-resolved studies of the kinetics of phase transitions [1]. Highlights in this history of the subject are, with respect to theory, the evaluation by Langer, Bar-on, and Miller of the effects of nonlinearities in the process of spinodal decomposition [2], which is the mode of phase separation of a mixture with the critical composition, the reworking by Langer and Schwartz of the classical theory of nucleation and growth, which is the phase-separation mode of off-critical metastable mixtures in order to take critical slowing down into account [3], and the recognition by Siggia of the crucial importance, in fluid systems, of hydrodynamic interactions [4]. Noteworthy experimental efforts are the observation of hydrodynamic effects during spinodal decomposition by Chou and Goldburg [5], measurement of the cloud points (metastability limits) of near-critical mixtures of Howland, Wong, and Knobler [6], and the extensive studies of the phase-separation kinetics of off-critical mixtures by Wong and Knobler [7]. As a natural extension of earlier work on the effect of shear flow on equilibrium critical-point phenomena [8], in the mid 1980s theorists began to consider phase separation under shear Theories of spinodal decomposition under shear predicted strongly anisotropic growth of the domains of the new coexisting phases, with the characteristic domain size in the flow direction increasing with a stronger time dependence than the size in the direction perpendicular to the flow [9]. Other theories predicted the suppression of the phase separation of metastable mixtures under shears strong enough to rupture the nucleating clusters, while weaker shears might speed the process up by inducing coalescence of clusters [10]. These topics are currently being studied experimentally. Recent experiments performed with mixtures of simple liquids have investigated the effects of shear on spinodal decomposition [11] and nucleation [12,13]. Shear effects on spinodal decomposition have also been studied in polymer [14] and micellar [15] solutions.

Under typical experimental conditions, the size of the concentration domains during the phase separation of liquid mixtures is of the order of 1–10 μm. Onuki has pointed out that structure on such a mesoscopic length scale is small enough still to be treated by continuum mechanics, but large enough to introduce significant stresses which would not be present in the homogeneous equilibrium mixture [16]. Thus the conceptually clean binary mixture of simple liquids can furnish an example of a rheologically complex fluid. Onuki's theory predicts that a liquid mixture undergoing phase separation under a steady shear tends toward a stationary state in which domain growth is balanced by the breaking up of large domains by the shear. The mechanical energy expended in the deformation of the domains against the capillary forces due to interfacial tension is lost when the domains break, so the continuous breaking of domains is macroscopically equivalent to viscous dissipation. Onuki gave a rough calculation of the effective viscosity $\Delta\eta$ of the domain-breakup process. Surprisingly, $\Delta\eta$ can be significant even though the interfacial tension is small

near the critical point. The theory predicts $\Delta\eta/\eta_0 \approx 1$, where η_0 characterizes the viscosity of the simple, homogeneous mixture without the effect of the domains.

Few experimental studies of the rheological behavior of phase-separating liquid mixtures have been reported. As far as we are aware, our preliminary report [17] and recent short paper [18] report the only results obtained with mixtures of simple liquids. We know of only one other related experiment, namely a recently reported measurement of extremely large viscosity enhancements in a polymer mixture simultaneously undergoing phase separation and gelation [19].

In this report, we describe measurements of the stress in flowing, phase-separating liquid mixtures made by observing the motion of a macroscopic body suspended in the mixtures. In the present work, the body is a disk that executes free oscillations. The fact that the resulting shear flow is oscillatory adds considerable complexity to the problem, but it also allows us to observe another important rheological attribute of these systems, namely viscoelasticity. A future paper will report the rheological behavior we see when the mixtures are subjected to steady shear flows imposed by a rotating cylinder.

This paper is organized as follows. Section II contains a description of our apparatus, sample preparation, and experimental procedure. Also included here is a full account of the working equation we use to calculate the viscosity and elastic shear modulus of a viscoelastic fluid from the measurable quantities that characterize the disk's motion. As far as we are aware, this material has not appeared elsewhere in the literature. Our results and analysis of experiments performed with a critical mixture of isobutyric acid and water appear in Sec. III. These results have already been reported in a short paper [18]. Here we give a much more detailed account of the application of a theory developed by Doi and Ohta to these measurements [20]. We also give predictions of their theory in regimes of shear rate and frequency not accessible with our viscometer. Section IV contains measurements of two off-critical mixtures, one rich in isobutyric acid and one rich in water. We compare the rheological behavior of these mixtures with the behavior of ideal emulsions. Our conclusions, including some speculative discussion of two unresolved puzzles posed by our experiments for off-critical mixtures, are the content of Sec. V.

II. EXPERIMENTAL DETAILS

A. Oscillating-disk viscometer, sample preparation, and procedure

The measurements are made with an oscillating-disk viscometer designed by Kestin and co-workers [21] and previously used to measure the viscosity of liquid toluene [22]. Figure 1 shows the instrument in an earlier configuration in which a thin disk is positioned between closely spaced fixed plates. In the present experiments, we use a squatter disk of radius $R_d = 25.41$ mm and thickness $2h = 10.16$ mm. Also, the spacing between the fixed plates and the disk has been increased to about 7 mm, sufficient to allow us to neglect the effect of the

plates on the fluid velocity around the disk. The disk is suspended from a torsion wire with a length of about 260 mm and a diameter of about 0.25 mm. The disk is made of Hastelloy C-276 for resistance to corrosion. The suspension wire is made of a 92%-Pt–8%-W alloy which yields high reproducibility of the rest position and low internal friction. The disk carries a small mirror on a long, thin stem. The disk and the assembly which supports the suspension wire are contained within a pressure vessel. The volume of the pressure vessel is about 1.3 l; this entire volume is filled with the fluid under study. A window in the vessel wall near the base of the instrument allows us to observe the disk's motion by monitoring a laser beam reflected from the mirror. We set the disk
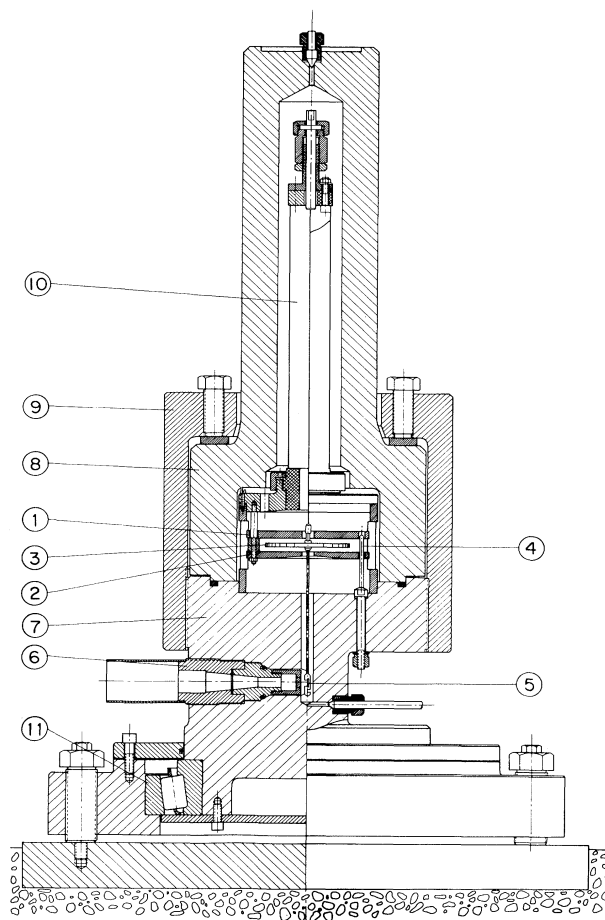

FIG. 1. The viscometer. The disk 3 is positioned between two fixed plates 1 and 2. The torsion wire from which the disk is suspended is carried by a column 10. A mirror 5 is attached to the disk by means of a long cylindrical stem. The lower part of the viscometer body 7 holds a sapphire window and its housing 6 and a thermowell 4 which contains a thermistor. The upper part of the viscometer body 8 defines the cavity occupied by the sample. The sample comes into contact with pressurized nitrogen gas near the port at the top of the instrument. The upper and lower parts are held together by a cap 9 which contains a ring of bolts. The seal is made by an O ring. The viscometer rests in a conical bearing 11 which allows us to set the disk into motion by rotating the instrument through a small angle.

into motion by rotating the viscometer through a small angle about an axis coincident with the suspension wire, then returning the instrument to its original position after a delay of about half of the disk's oscillation period. In the absence of a fluid (that is, when the vessel has been evacuated), the disk oscillates with negligible damping at its natural frequency ω_0 set by its moment of inertia and the stiffness of the suspension wire. The corresponding period *in vacuo* $T_0 = 2\pi/\omega_0$ is 3.891 s at 25 °C.

Good thermal stability near room temperature is required for these experiments. In order to thermostat the viscometer, we have placed it in inside an insulated, airtight box. The air inside the box is circulated around the instrument and through a chamber containing a liquid-cooled heat exchanger and a heat source. Air-temperature stability of 20 mK over a duration of several hours can be attained. Because of the large thermal mass of the viscometer, over such times its temperature remains constant to within a few mK. In the experiment, we vary the pressure at constant temperature; the exact value of the temperature is not important as long as it remains constant during the experiment. The liquid sample comes into contact with nitrogen gas near the top of the pressure vessel. Simple techniques allow us to measure and control the gas pressure P over the range $0.1 < P < 10$ bar with an accuracy of 0.01 bar.

Concentration gradients can develop in liquid mixtures close to the consolute point due to the enhanced effects of sedimentation and thermal diffusion [23,24]. In order to keep the concentration uniform, we stir the sample by pumping it from the bottom to the top of the viscometer through an external pump. This procedure is carried out routinely, usually at intervals of several days or whenever consideration of the reproducibility of the measured viscosities suggests that the local concentration of the sample in the vicinity of the disk may have changed.

In the case that the disk is surrounded by a viscous fluid whose properties are constant in time, the free motion of the disk is of the form

$$\alpha(t) = \alpha_0 \exp(-\Delta\omega t)\sin(\omega t) . \qquad (1)$$

Here $\alpha(t)$ is the position angle of the disk at time t, α_0 is the initial amplitude of the oscillation, ω is the frequency, and Δ is the logarithmic decrement, or damping. The period $T = 2\pi/\omega$ and damping Δ are related to the fluid properties through a working equation which we discuss below. As an example, when surrounded by a Newtonian fluid of viscosity $\eta = 2.6$ mPa s and density $\rho = 1.0$ g/cm^3 (values typical of near-critical isobutyric acid and water mixtures), the values of the period and damping are approximately $T = 3.963$ s and $\Delta = 0.0203$. This value of Δ describes a motion in which the oscillation amplitude decays by a factor of $1/e$ in about eight oscillations. Note that the period and damping are comparably affected by the fluid in the sense that the relative change $(T - T_0)/T_0$ of the period from its value in vacuo, 0.0185 in this example, is roughly equal to the value of the damping.

We determine the oscillation period T and the damping Δ by a method that requires only the measurement of the time intervals between the detection of the reflected laser

beam at several fixed positions [25]. Figure 2 shows a sketch of the arrangement. The mirror 1 is attached to the disk. A photodiode detector 2 is located at the beam's rest position. Another "offset" detector 3 is located at an arbitrary angle. Signals generated by the passage of the beam across the detectors are shaped and amplified by an amplifier 4 and then fed into two quartz-crystal timers 5 and 6. The timers are configured so that timer 5 records the time intervals between successive detections of the beam at the rest position, while timer 6 records the time intervals between the detection of the beam at the rest position and its subsequent detection at the offset position. We denote these latter intervals by τ_i, where the subscript refers to cycle number. The τ_i are short initially when the amplitude of the disk's motion is large, but they increase as the motion decays, with the last of the recorded τ_i tending toward $T/4$ as the amplitude of the oscillation becomes just sufficient for the beam to reach offset detector 3. Thus the intervals measured by timer 5 directly furnish the half-period $T/2$, while the rate of increase of the intervals τ_i allows the computation of the damping Δ according to

$$2\pi\Delta = \frac{\ln[\sin(\omega\tau_j)/\sin(\omega\tau_k)]}{j - k + (\tau_j - \tau_k)/T} \qquad (2)$$

for any pair of intervals τ_j and τ_k and $\omega = 2\pi/T$. In practice, one has to apply small corrections to both sets of measured time intervals in order to account for the finite width of the laser beam and for the fact that detector 2 generally is not located exactly at the beam's rest position. To do this, we use a procedure similar to the one described in Ref. [25]. Reproducibility at the level of 0.05 ms and 5×10^{-6}, respectively, is readily obtained for the measurements of T and Δ by this method.

In the present experiments, we consider processes during which the fluid properties change in time, so that the disk undergoes a more complicated motion than that de-
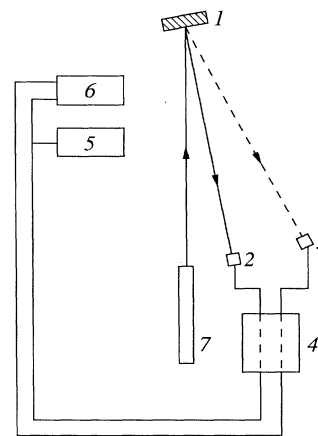

FIG. 2. Schematic diagram of the arrangement to detect the motion of the disk. The mirror 1 is attached to the disk and oscillates about an axis perpendicular to the plane of the paper. Light reflected from the laser 7 passes over detectors 2 at the rest position and 3 at an offset position. The signals are shaped by an amplifier 4 and fed into two quartz-crystal timers 5 and 6.

scribed by Eq. (1). We assume, however, that Eq. (1) remains a good approximation to the disk's motion over each oscillation cycle, and we speak of the "cycle-by-cycle" values of the period T_i and damping Δ_i obtained from the successively measured period intervals T_i and the application of Eq. (2) with $T=T_i$, $\tau_j=\tau_i$, and $\tau_k=\tau_{i+1}$. By solving the instrument's working equation with T_i and Δ_i as inputs, we obtain cycle-by-cycle values of the changing fluid properties. These we refer to the time that locates the midpoint of the ith cycle.

Not shown in Fig. 2 is a second offset detector on the side of the rest position opposite to that of the offset detector 3. This detector records a second set of time intervals analogous to the intervals τ_i measured at detector 3, and a parallel treatment of them gives a second set of cycle-by-cycle values of the fluid properties. Because the detections at the second offset detector occur at times displaced from the times of detection at detector 3 by approximately one half of an oscillation period, the times of reference for the second set of fluid properties interpenetrate the reference times of the first set. Thus by using two offset detectors, we are able to measure the rheological properties of the fluid as functions of time with $T/2\approx 2$ s as the time resolution.

Mixtures of isobutyric acid (IBA) and water are particularly suitable for these experiments. For example, the components have similar densities, so that the effects of gravity on the process of phase separation can be kept small [26]. Also, the pressure-quench technique (described below) works particularly well with these mixtures [7]. We prepared samples from distilled, degassed water and IBA as supplied commercially with a stated purity of 99%. We did not attempt further purification of the IBA because of the large quantities required. However, care was taken to ensure that only inert gases came into contact with the samples during their preparation and transfer into the viscometer. The compositions of the mixtures were determined by weighing the components on a large double-pan balance. We performed experiments with three samples: a sample at the critical composition, an IBA-rich sample, and a water-rich sample. The compositions, expressed as mass fractions of IBA, are 0.388, 0.426, and 0.343, respectively.

The pressure-quench technique [7,27] for inducing phase separation in liquid mixtures is based on the pressure dependence of the critical temperature $T_c(P)$. For IBA plus water [7],

$$\frac{dT_c}{dP}=-54 \text{ mK/bar} . \tag{3}$$

We assume that the dependence of the critical concentration on the pressure may be neglected, and that the separation temperatures of the off-critical coexistence mixtures $T_{cx}(P)$ have the same dependence on pressure as the critical temperature: $dT_{cx}/dP=-54$ mK/bar. In the experiments, we work at a fixed temperature T_d of the disk. (The subscript has been added to avoid confusion with the period T. In the subsequent parts of the paper, where it will not be necessary to refer to both quantities within the same section, we shall use the same symbol T

to denote either the temperature or the period.) We define the critical pressure $P_c(T_d)$ [or the phase-separation pressure $P_{cx}(T_d)$] as the pressure at which $T_c(P)=T_d$ [or $T_{cx}(P)=T_d$]. At pressures above P_c or P_{cx}, the sample is in a one-phase equilibrium state. Phase separation is induced by sudden depressurization to a final pressure P_f below P_c or P_{cx}. Because of adiabatic expansion, the sample cools slightly, but this effect is small in IBA-plus-water mixtures for which the adiabatic thermal pressure coefficient $(\partial T_d/\partial P)_S$ is small. Thus the depressurization to the final pressure P_f is equivalent to a temperature quench of depth $Q=(P_c-P_f)|dT_c/dP|$ (or this expression with P_{cx} replacing P_c in the case of an off-critical mixture). We shall routinely specify the depth of a pressure quench as the depth of the equivalent temperature quench. The values of the quench depth Q given below include a correction for adiabatic cooling based on an estimate of 3 mK/bar for $(\partial T_d/\partial P)_S$ [7].

The viscometer's metallic walls and its placement inside the thermostat make a direct determination of P_c or P_{cx} by visual observation of the sample impossible. It is therefore necessary for us to infer P_c or P_{cx} from the behavior of the viscosity. We restrict the viscosity measurements made at steady pressures in the one-phase region to pressures at least 1 bar above P_c or P_{cx}. This practice is necessary because we often observe that the viscosities measured at constant pressure begin to drift slowly at a rate of the order of 1% per hour upon our setting of the pressure to a lower value. We attribute this behavior to incipient phase separation of the samples at locations away from the disk due to temperature or concentration gradients which are difficult to eliminate completely in an instrument of this size. In the experiments on the critical mixture we determine the critical pressure P_c by measuring the viscosity in the one-phase region P_c+1 bar $<P<P_c+8$ bar as a function of pressure, then fitting these data with an expression of the form [17]

$$\eta(P)=A_P\left[\frac{P-P_c}{P_c}\right]^{-\psi} . \tag{4}$$

Here A_p and P_c are treated as fitting parameters and the critical exponent ψ has the value 0.040 [17,28–30]. We find that this procedure locates $P_c(T_d)$ within a statistical resolution of about 0.1 bar, which is equivalent to about 5 mK. This value may therefore be taken as the uncertainty in the values for the quench depths Q we report for the experiments performed on the critical mixture.

For later computations, it is convenient to rewrite Eq. (4) in the form $\eta=A\epsilon^{-\psi}$, where the equivalent reduced temperature $\epsilon=(T_d-T_c^0)/T_c^0$ replaces the reduced pressure $(P-P_c)/P_c$. Here T_c^0 denotes the critical temperature referred to zero pressure via Eq. (3) in the form

$$T_c^0=T_d+\frac{dT_c}{dP}P_c(T_d) . \tag{5}$$

From a comparison of several sets of data, fitted separately by Eq. (4), we arrive at $A=(2.00\pm0.02)$ mPa s with $T_c^0=299.80$ K. This value for T_c^0 is about 1 K higher than is typically reported for carefully purified critical

samples of IBA plus water under its vapor pressure. We suppose that the discrepancy is due to impurities in our sample and that it has no important consequences for our experiment. This is confirmed by the observation that our value of $A = (2.00 \pm 0.02)$ mPa s is in agreement with the value obtained by other investigators [28,31,32]. Actually, the viscosity amplitude A is expected to depend on temperature [28]; the value given here applies for temperatures near $T_d \approx 26.8\,°C$.

Viscosity data taken in the one-phase region of an off-critical mixture may also be represented by an expression of the form Eq. (4). In this case, however, one must replace P_c with a parameter P_{ps} which is not the phase-separation pressure P_{cx}, since in fact the viscosity of an off-critical mixture remains finite in the vicinity of P_{cx}. Instead, $P_{ps} < P_{cx}$ is a pressure inaccessible to one-phase equilibrium states which we may call the pseudospinodal pressure [32,33]. The physical significance of P_{ps} and its relation to P_{cx} are not clear, so although we determine P_{ps} in the manner described, we use a different approach to fix P_{cx}. Namely, we make a series of viscosity measurements during which we drop the pressure from a fixed initial value $P_i \approx P_{cx} + 2$ bar to a lower final pressure P_f. The pressure is returned to P_i after about ten oscillation cycles. A lower and lower final value is chosen for P_f as we progress through the series. Initially, at the final pressure P_f the sample is still in the one-phase region, and the viscosities measured at P_f show a weak increase with decreasing P_f due to critical enhancement. Eventually, however, we notice a marked break in the slope of a plot of $\eta(P_f)$ versus P_f which we attribute to enhancement of the viscosity by domains formed during phase separation. According to this interpretation, we identify the phase-separation pressure P_{cx} with the pressure where we see the abrupt change of the slope. This procedure locates P_{cx} within a resolution of about 0.3 bar, so that the values of the quench depths reported for the experiments on the two off-critical mixtures are uncertain by about 15 mK.

An important parameter characterizing the off-critical mixtures is the difference $T_c - T_{cx}$ of the critical and phase-separation temperatures (at the same pressure). In principle, this information is furnished by the measurements (at the same temperature) of P_c and P_{cx} for the critical and off-critical samples. In fact, however, we find that the measured values of P_c and P_{cx} for our three samples are not consistent with coexistence-curve information on the IBA-plus-water system taken from the literature. We assume these inconsistencies are due to impurities which may be present in the different samples in different concentrations. Another problem is that our samples are effectively open systems, since following a quench we repressurize the viscometer with fresh nitrogen gas. This practice may contribute to the large drift rates (for example, about -4 mK per day in the case of the critical sample) of the critical and phase-separation temperatures that we observe. Therefore, when the value of $T_c - T_{cx}$ is required in the analysis of the behavior of the off-critical mixtures, we regard it as a parameter determined by the sample composition and calculate it

from an expression for the coexistence curve of IBA plus water [32,34]. This expression appears in Table I. From it we calculate $T_c - T_{cx} = 61$ mK for the water-rich sample (IBA mass fraction 0.343) and $T_c - T_{cx} = 32$ mK for the IBA-rich sample (IBA mass fraction 0.426).

The procedure for quench measurements in the critical and off-critical mixtures is similar. We set the disk into motion while the sample is in the one-phase region at an initial pressure P_i from 1 to 2 bar above P_c or P_{cx}. After the disk completes several cycles, we drop the pressure to the desired final value P_f. We monitor the motion of the disk for about 40 s during the phase-separation process that follows. We then raise the pressure to a high value, typically several bar above the initial pressure P_i, and allow the system some time to reequilibrate. By comparing the values of the viscosity measured before and after the quench experiment, we judge whether remixing is required.

The samples become very turbid during phase separation, but the optical method used to observe the disk's motion requires that the samples remain transparent in the vicinity of the window and mirror. To solve this problem, shortly before a quench we apply a current pulse to a small electric heater cemented to the viscometer's surface just behind the mirror. This warms the region near the mirror and window slightly so that the sample thereabout remains sufficiently clear during the quench. The long length of the mirror stem (about 100 mm) and the fixed plates around the disk prevent this procedure from having a measurable effect on the samples in the vicinity of the disk during the quench measurement. The method is effective only for quenches that are not too deep. The quench-depth limit for our experi-

TABLE I. Properties of coexisting phases of near-critical IBA-plus-water mixtures.

Critical temperature[a]	$T_c = 299.80$ K
Critical composition[b]	$X_c = 0.388$
(IBA mass fraction)	
Reduced temperature[c]	$\epsilon = (T_c - T)/T_c$
Coexistence curve[d]	$X_U - X_L = g_1 \epsilon^{0.324}$; $g_1 = 1.44$
	$X_U + X_L = 2(X_c + g_2 \epsilon)$; $g_2 = 2.03$
Correlation length[e]	$\xi^- = \frac{1}{2}\xi_0 \epsilon^{-0.63}$; $\xi_0 = 0.362$ nm
Mass diffusivity[f]	$D^- = k_B T_c / 6\pi \eta \xi^- = (6.0 \times 10^{-10}\ m^2/s) \epsilon^{0.67}$
Interfacial tension[g]	$\Gamma = \Gamma_0 \epsilon^{1.26}$;
	$\Gamma_0 = k_B T_c / 2.6(\xi_0)^2 = 1.21 \times 10^{-2}$ N/m
Viscosity[h]	$\eta_{(U,L)} = (\eta^B \pm A'\epsilon^{1/3})\epsilon^{-0.04}$;
	$\eta^B = 1.89$ mPa s $A' = 2.60$ mPa s

[a]These measurements.
[b]Reference [35].
[c]T stands for the equivalent final temperature after a pressure quench: $T_c - T = \Delta T + Q$, where $\Delta T = T_c - T_{cx}$ is 32 mK for the IBA-rich mixture and 61 mK for the water-rich mixture.
[d]References [32] and [34].
[e]Reference [31].
[f]Where $\eta = (2.0$ mPa s$) |\epsilon|^{-0.04}$ is identified with the viscosity of the critical mixture in the one-phase region.
[g]Reference [36].
[h]References [32] and [37]. The upper phase (IBA rich) takes the plus sign.

ments on the critical mixture is about 70 mK; beyond this the reflected beam becomes too faint and diffuse for reliable detection. The limit for the off-critical mixtures is about 200 mK.

Measurements during which we make a jump between equilibrium states in the one-phase region test the viscometer's ability to yield the rheological properties as functions of time and also assure us that the sudden pressure change introduces no spurious instrumental effects. Figure 3 shows an example of a run of measurements performed in the one-phase region of the critical mixture. The viscosity at constant temperature $T_d = 26.76\,^\circ$C is shown as a function of pressure. Data represented by circles were obtained in measurements during which the pressure was steady. A fit of Eq. (4) to these data yields the amplitude $A_P = 2.69$ mPa s and critical pressure $P_c = 3.27$ bar. The viscosity value represented by a diamond was calculated from the time-averaged values of the period and damping which we measured following a sudden decrease of the pressure from 4.80 to 3.61 bar. The agreement with the extrapolation of the fit made to the data taken at steady pressures is excellent. With adiabatic cooling taken into account, the pressure jump is equivalent to a jump between an initial state 93 mK above the critical temperature to a final state 14 mK above the critical temperature. Figure 4 shows the rheological properties during the pressure-jump experiment as functions of time which were calculated from the cycle-by-cycle values of the period and damping. The figure shows that the measured viscosity η becomes constant at its final value within one oscillation cycle. This indicates that we need not deconvolute an instrumental response from the time-dependent rheological properties inferred from the disk's motion during the phase-separation experiments. The quantity G, which is defined in the following section, is the elastic shear modulus. A finite
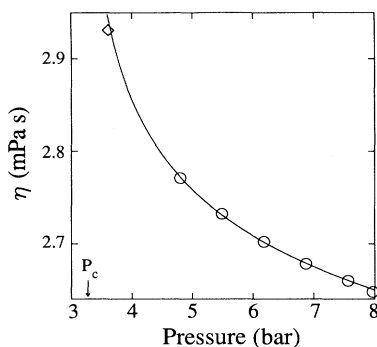

FIG. 3. Viscosity η of the critical mixture of IBA and water at constant temperature as a function of the pressure P. The curve is a fit of Eq. (4) to the data represented by circles; the pressure remained steady during each of these measurements. The point represented by a diamond was measured after suddenly decreasing the pressure from 4.80 to 3.61 bar. The fitted value of the critical pressure is $P_c = 3.27$ bar, so that the final pressure is equivalent to a temperature 14 mK above the critical point. The viscosity and elastic shear modulus measured during the pressure-jump experiment as functions of time appear in Fig. 4.
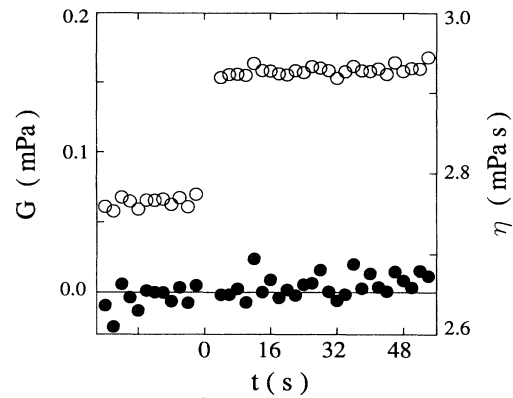

FIG. 4. Viscosity η (open circles) and elastic shear modulus G (closed circles) of the critical mixture of IBA and water as functions of time t measured during the pressure-jump experiment illustrated in Fig. 3. The pressure was dropped to the lower value at time $t = 0$.

value for G implies that a fluid is viscoelastic. In Fig. 4, the measured values of G are scattered about zero, as should be the case here since in its equilibrium states the sample is a simple Newtonian fluid [38].

B. Working equations for Newtonian and viscoelastic fluids

The working equation connecting the period and damping of the disk's motion with the properties of the fluid is found by solving the Navier-Stokes equation for the velocity of the fluid around the disk subject to a no-slip boundary condition on the surface of the moving disk. An exact solution to this problem is not available, but an accurate approximation has been found in the case where the fluid is Newtonian [39–41]. A most important contribution was made by Newell, who evaluated the large edge effect [39]. More recently, Nieuwoudt, Kestin, and Sengers reviewed the theory of oscillating-body viscometers and investigated the possibility of determining both the viscosity and the density of a Newtonian fluid from the damped oscillating motion of a disk suspended in the fluid [40]. In the present work, we generalize the working equation appropriate to a Newtonian fluid by treating the viscosity as a complex number. In this way we derive a working equation which allows us to determine both the viscosity η and the elastic shear modulus G of a viscoelastic fluid. We present the derivation and the result in some detail because in this way the quantity G can be precisely defined and because our result constitutes an improvement of the working equation presently to be found in the literature for the measurement of the properties of viscoelastic fluids [42].

We begin with the result appropriate for a Newtonian fluid. The calculation is most naturally carried out by Laplace transform methods, and one obtains a complex working equation in the form of a condition satisfied by the Laplace transform of the time-dependent viscous torque acting on the disk. The result is [39–41]

$$s^2+1+\frac{\rho\delta}{\bar{\rho}h}\left\{\left[1+4\frac{h}{R_d}\right]s^{3/2}+Bs\left[\frac{\delta}{R_d}\right]\right.$$

$$\left.+Cs^{1/2}\left[\frac{\delta}{R_d}\right]^2\right\}=0 \ , \qquad (6)$$

where the complex number $s=(-\Delta+i)T_0/T$ contains the period and damping, and the viscosity and density are contained in the boundary layer thickness $\delta=(\eta/\omega_0\rho)^{1/2}$, which characterizes the thickness of the region of appreciable fluid flow. The radius of the disk is R_d and its half-thickness is h. The coefficients B and C are geometrical constants:

$$B=\frac{16}{3\pi}\left[\frac{4\pi}{\sqrt{27}}-1\right]+6\frac{h}{R_d}, \quad C=\frac{17}{9}+\frac{3h}{2R_d} \ , \qquad (7)$$

and $\bar{\rho}=8.80$ g/cm^3 is the density of the material from which the disk is made. Equation (7) includes the effects of the complicated fluid-flow pattern in the vicinity of the disk's edges. It is valid in the case that $\delta\ll h\ll R_d$. A typical value for δ is 1 mm.

The complex equation (6) represents a coupled pair of real equations. The quantities related by them are the two measured parameters of the disk's motion T and Δ, two fluid properties η and ρ, and the instrumental constants R_d, h, $\bar{\rho}$, and $\omega_0=2\pi/T_0$. Since we consider the fluid density ρ to be given, the two equations contain a single unknown, namely the viscosity η. The equations are therefore overdetermined, which implies the existence of a consistency relation between the period T and the damping Δ. That is, it is possible to express T as a function of Δ, the fluid density ρ, and instrumental constants. A rough approximation to this relation is the simple expression $T/T_0\approx1+\Delta$, for which we gave a numerical example above. The full form of the consistency relation is given in implicit form in the Appendix. We find that the full form of the consistency relation is quite accurate, in that values for T calculated from it agree with the measured values to within 0.2 ms when T and Δ are measured while the IBA-plus-water mixtures are in their equilibrium states as Newtonian fluids. However, during the process of phase separation that occurs after a quench of the samples into their regions of immiscibility, we find that the measured values of the period may be as much as 10 ms smaller than the value expected on the basis of the consistency relation and the measured damping. Our interpretation of this behavior is that a liquid mixture undergoing phase separation behaves as a viscoelastic fluid. We suppose that the interfaces between the concentration domains that form during phase separation have a finite interfacial tension, so that energy is required for the stretching of the domains that may occur in a shear flow [16]. In this way, the liquid may exert a restoring force on the disk which adds with the restoring force supplied by the torsion wire. The net effect is to decrease the period to a lower value than the one that would result in the absence of elasticity in the fluid.

In order to deduce quantitative information about the phase-separating mixtures from the period and damping measurements, we need a working equation linking the measured quantities with the properties of a viscoelastic fluid. In a calculation from first principles, we would return to the fluid-velocity boundary value problem and consider the revised equations of motion of the fluid that result when the stress and fluid-velocity fields are related by a constitutive equation appropriate for a viscoelastic fluid. A much simpler approach is possible in the case that the shear flow has a sinusoidal dependence on time: beginning with Eq. (6), the working equation of a Newtonian fluid, we generalize it by replacing the unknown real viscosity η by an unknown complex viscosity $\eta^*=\eta'-i\eta''$ to yield

$$s^2+1+\frac{\rho\delta^*}{\bar{\rho}h}\left\{\left[1+4\frac{h}{R_d}\right]s^{3/2}+Bs\left[\frac{\delta^*}{R_d}\right]\right.$$

$$\left.+Cs^{1/2}\left[\frac{\delta^*}{R_d}\right]^2\right\}=0 \ , \qquad (8)$$

where $\delta^*=(\eta^*/\rho\omega_0)^{1/2}$. This complex equation represents two real equations in the unknown quantities η' and η'' which are determined by the now independent quantities T and Δ.

The physical meaning of the complex viscosity becomes clear when we write down the equation for the stress in terms of η' and η''. Specifically, we consider a simple shear flow in which the fluid viscosity v is given by

$$v_x(t)=S(t)y, \quad v_y=0, \quad v_z=0 \ , \qquad (9)$$

where $S(t)$ is the shear rate. In the case of a Newtonian fluid, the shear component of the stress tensor is given by $\sigma_{xy}(t)=\eta S(t)$ for arbitrary $S(t)$. On the other hand, the description of a viscoelastic material by a complex viscosity is possible when $S(t)$ has the form

$$S(t)=S_0\exp(-\Delta\omega t)\cos\omega t \ , \qquad (10)$$

where, in general, the initial shear-rate amplitude S_0 as well as the phase of the oscillation may vary with position. (An undamped flow, $\Delta=0$, is of course an allowed special case.) The complex viscosity η^* describes a viscoelastic material for which the shear component of the stress tensor is given by

$$\sigma_{xy}(t)=S_0\exp(-\Delta\omega t)(\eta'\cos\omega t+\eta''\sin\omega t) \qquad (11)$$

when Eqs. (9) and (10) hold. By defining $S^*(t)=S_0\exp[(-\Delta+i)\omega t]$, we can write Eq. (11) as $\sigma_{xy}(t)=\text{Re}[\eta^*S^*(t)]$, which has the same form as the Newtonian relation $\sigma_{xy}(t)=\text{Re}[\eta S^*(t)]$. As a result, the fluid-velocity field around the oscillating disk executed by a viscoelastic fluid for which the stress is given by Eq. (11) differs from that of a Newtonian fluid only by phases. Therefore, the working equation relating (T,Δ) with (η',η'') appropriate to such a fluid is found by substitution into Eq. (6) of $\eta^*=\eta'-i\eta''$ for η with no change in the form of Eq. (6), as we have assumed.

We can rewrite Eq. (11) in an equivalent but physically more suggestive form. We begin with the identity

$$e^{-\Delta\omega t}\sin\omega t=\omega(1+\Delta^2)\int_{t_0}^{t}e^{-\Delta\omega t'}\cos\omega t'dt'$$

$$+\Delta e^{-\Delta\omega t} \cos\omega t \ , \qquad (12)$$

where $\tan(\omega t_0)=\Delta$ defines the lower integration limit t_0. Equation (11) then becomes

$$\sigma_{xy}(t)=\eta S(t)+G\int_{t_0}^{t}S(t')dt' \ , \tag{13}$$

where Eqs. (9) and (10) are assumed to apply and where η and G are related to η' and η'' by

$$\eta=\eta'+\Delta\eta'', \quad G=\omega(1+\Delta^2)\eta'' \ . \tag{14}$$

The first term of Eq. (13) represents ordinary viscous action. Henceforth we shall refer to the combination $\eta=\eta'+\Delta\eta''$ as the viscosity of the viscoelastic fluid; it differs only slightly from the real part of the complex viscosity η^* since Δ is small. Since $S(t)$ is the shear rate, or velocity gradient, its time integral is the gradient of relative displacement, so we may identify the integral in Eq. (13) with the shear strain present in the viscoelastic material at time t. [The choice $\tan(\omega t_0)=\Delta$ for the initial time t_0 when the strain is taken to be zero insures that the strain tends to zero with the decaying shear rate $S(t)$ at long times.] The combination $G=\omega(1+\Delta^2)\eta''$ is therefore the effective elastic shear modulus of the fluid. Throughout the rest of this paper, we will be concerned with the measurement and prediction of the rheological properties η and G of phase-separating liquid mixtures.

For computations, it is often convenient to work with the explicit expressions for the real and imaginary parts of Eq. (8). The notation required is somewhat cumbersome, so we give these expressions in the Appendix.

III. CRITICAL MIXTURE

A. Measurements and analysis for damped oscillatory shear

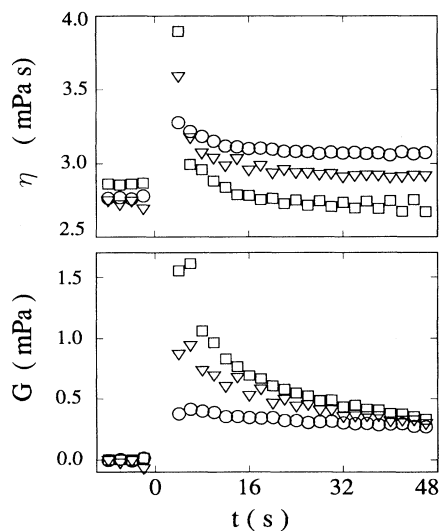Figure 5 shows the results of three typical quench measurements in which the final pressures are equivalent to

FIG. 5. Viscosity η and elastic shear modulus G of the critical mixture as functions of time during spinodal decomposition following quenches to final temperatures below T_c. The symbols $\bigcirc$, $\triangledown$, and $\square$ correspond to quenches of depths 11, 19, and 64 mK, respectively.

temperatures 11, 19, and 64 mK below the critical temperature. The quench occurs at time $t=0$. The earliest post-quench values of the viscosity η and the elastic shear modulus G are referred to time $t=4$ s; they derive from the period and decay of the disk's motion that occurred between $t=2$ and 6 s. The values of η and G at this earliest time increase with quench depth. As functions of time, η and G decrease, with the rapidity of the decrease at early times increasing with the quench depth. The values of the viscosity at the earliest time after the deeper quenches appear discontinuously high compared with their subsequent values at times $t \geq 6$ s. Many quench experiments have convinced us that this behavior is reproducible and systematic. The time dependence of G is smoother. The viscosity becomes constant after four or five disk oscillations at a final value that decreases with increasing quench depth. The elastic modulus G continues to decrease at all measured times, but near the end of the measurement its rate of decrease becomes small and its value appears to become independent of the quench depth.

We denote by η_0 the value at which the viscosity becomes constant. For the experiments shown in Fig. 5, we have $\eta_0=3.07$, 2.91, and 2.72 mPa s corresponding to the quench depths $Q=11$, 19, and 64 mK, respectively. The values of η_0 are comparable to the values of the viscosity one might expect for this system in the absence of an enhancement by concentration domains. For example, as is discussed below Eq. (5), the viscosities of the one-phase equilibrium states at equal distances Q above the critical point may be calculated as $A(Q/T_c^0)^{-0.040}$ with $A=2.00$ mPa s and $T_c^0=299.80$ K. This expression gives 3.01, 2.94, and 2.80 mPa s for the three values of Q. Also pertinent is a comparison of η_0 to $\eta_U(Q)$ and $\eta_L(Q)$, the viscosities of the coexisting upper and lower phases to which the system would eventually evolve were the phase-separation process allowed to continue. However, we have not measured the viscosities of the coexisting phases, nor are many such measurements to be found in the literature. In the discussion of the measurements on the off-critical mixtures we shall give a formula from which we estimate η_U and η_L, and we find that the estimated values of η_U and η_L bracket η_0. In the case of the critical quench of depth 64 mK, for example, we estimate $\eta_U \approx 2.9$ mPa s for the viscosity of the IBA-rich upper phase and $\eta_L \approx 2.4$ mPa s for the viscosity of the lower phase. It therefore seems reasonable to identify the contribution of the domains $\Delta\eta$ to the measured effective viscosity η as $\Delta\eta=\eta-\eta_0$ and regard η_0 as the background viscosity characteristic of the mixture in a homogenized state without domains. According to this interpretation, the relative enhancement of the effective viscosity by concentration domains $\Delta\eta/\eta_0$ can be as high as 0.4 at times just after the quench (see Fig. 6). This result is in agreement with Onuki's prediction of a relative enhancement of the order 1. However, his result $\Delta\eta/\eta_0 \sim 1$ describes a stationary state of constant effective viscosity which the system may attain at sufficiently long times when subjected to a steady shear flow [16]. In our experiments in which the shear flow is oscillatory, we measure $\Delta\eta/\eta_0 \sim 1$ only at the earliest
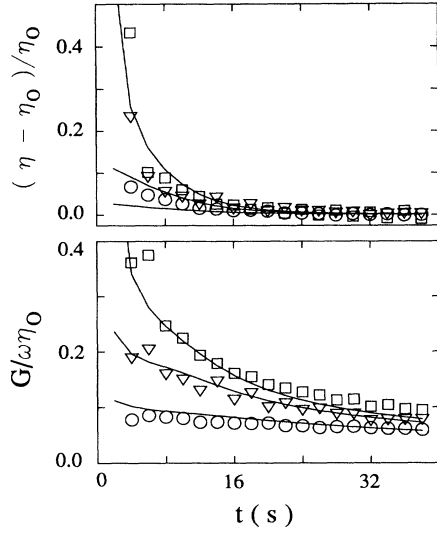
FIG. 6. Reduced interfacial viscosity $(\eta-\eta_0)/\eta_0$ and reduced elastic shear modulus $G/\omega\eta_0$ as functions of time t. The curves have been calculated from the theory of Doi and Ohta. Symbols have the same meaning as in Fig. 5.

times when $\Delta\eta$ is changing rapidly, and the long-time behavior is $\Delta\eta/\eta_0\rightarrow0$.

Doi and Ohta have developed a phenomenological theory that can describe the time dependence of the rheological properties of a phase-separating critical mixture undergoing time-dependent flows [20]. The interconnected concentration domains are thought of as a blend of immiscible liquids separated by an intricate interface. In a flow, the traceless part of the stress tensor of this system is given by

$$\sigma_{\alpha\beta}=\eta_0\left[\frac{\partial v_\alpha}{\partial x_\beta}+\frac{\partial v_\beta}{\partial x_\alpha}\right]-\Gamma q_{\alpha\beta} \ , \tag{15}$$

where Γ is the interfacial tension and the interface tensor $q_{\alpha\beta}$ is defined as [16,20]

$$q_{\alpha\beta}=\frac{1}{V}\int ds(n_\alpha n_\beta-\tfrac{1}{3}\delta_{\alpha\beta}) \ . \tag{16}$$

Here v is the macroscopic fluid velocity obtained by taking a coarse-grained spatial average of the microscopic flow in order to remove the intricate details that occur on the length scale set by the characteristic size of the domains. The first term of Eq. (15) represents the viscous stress associated with the macroscopic flow. Here, therefore, the viscosity η_0 represents the viscosity of the system apart from the contribution of the interfaces, and consequently corresponds to the experimentally defined quantity we have denoted by the same symbol. The second term of Eq. (15) introduces the effect of the domains in the form of the stress arising from deformations of their interfaces that may occur as the system flows. In the definition of $q_{\alpha\beta}$, n_α and n_β are components of the unit vector n normal to the interface. The integral is to be taken over all the interfacial surfaces within a

coarse-graining volume V whose linear dimensions are large compared to the domain size but small compared to the length scale of the macroscopic flow. By its construction, $q_{\alpha\beta}$ is traceless, so it vanishes in the case where the interface is, on the average, isotropically oriented.

Doi and Ohta have derived an equation of motion for the interface tensor $q_{\alpha\beta}$ in the form of a set of coupled differential equations among the tensor elements of $q_{\alpha\beta}$, the macroscopic velocity-gradient tensor $D_{\alpha\beta}$, and the interfacial area per unit volume q. In the case of the simple shear flow represented by Eq. (9), they take the form

$$\frac{dq_{xy}}{dt}=S(t)\left[\frac{q_{xy}^2}{q}-q_{xx}-\frac{q}{3}\right]-(c+k)\frac{\Gamma}{\eta_0}qq_{xy} \ , \tag{17}$$

$$\frac{dq_{xx}}{dt}=S(t)\left[\frac{q_{xy}q_{xx}}{q}+\tfrac{2}{3}q_{xy}\right]-(c+k)\frac{\Gamma}{\eta_0}qq_{xx} \ , \tag{18}$$

$$\frac{dq}{dt}=-S(t)q_{xy}-c\frac{\Gamma}{\eta_0}q^2 \ . \tag{19}$$

The component of the interfacial stress which affects the disk's motion is $-\Gamma q_{xy}$. A finite value for the component q_{xx} indicates a difference in the normal components of the stress [16]. The terms on the right in Eqs. (17)–(19) describe free streaming of the interface in the macroscopic shear flow. The remaining terms are phenomenological terms that enforce the decay of q_{xy}, q_{xx}, and q. The decay of q is according to the capillary-driven linear growth of the interconnected domains that occurs in the late stage of spinodal decomposition in fluids [4,5,7]. This can be seen by noting that the characteristic domain diameter $a(t)$ is related to the interfacial area per unit volume $q(t)$ by $a(t)\propto q^{-1}(t)$ [26], and that in the absence of a macroscopic flow $[S(t)=0]$, the solution of Eq. (19) is $q^{-1}(t)=q_0^{-1}+c(\Gamma/\eta_0)t$, where $q(t=0)\equiv q_0$ is the extent of the interface at some initial time. The second terms of Eqs. (17) and (18) describe the decay of the interface tensor according to the combined effects of the decay of q (that is, the decay of the interface itself) and relaxation of interfacial anisotropy by interfacial tension. The first of these processes involves the dimensionless constant c, which is known to be of the order 10^{-2} [7]. The relaxation of interfacial anisotropy is governed by the dimensionless constant k, about which we have no a $priori$ knowledge.

To apply the theory to our experiment, we consider the case where the shear rate is given by $S(t)=S_0\exp(-\Delta\omega t)\cos(\omega t)$. In doing so, we are treating the shear rate as given information and calculating the interface's resulting rheological response. In a more fundamental treatment, we would derive the shear rate by solving the fluid-velocity equations for the fluid whose constitutive equation included Eqs. (17)–(19). Furthermore, we consider the damping Δ and the frequency ω to be constants. We thus ignore here the time variation of Δ and ω, which, in the experiment, enable us to measure the time dependence of η and G. The values $\Delta=0.022$ and $\omega=1.58$ Hz we adopt are typical averages over time of the damping and frequency measured during quenches. For S_0, the initial shear-rate amplitude at the surface of

the disk, we adopt the value 7.9 s^{-1}. We arrive at this value from the assumption that the fluid-velocity gradient at the surface of the disk is the disk's velocity divided by the length $|\delta^*|$, where $\delta^* = (\eta^*/\rho\omega)^{1/2}$ is computed with a time-averaged value of the complex viscosity η^* measured during the quench. A simple spatial average has been taken to account for the dependence of the disk's linear velocity on the radial coordinate.

It is convenient to rewrite Eqs. (17)–(19) in dimensionless form. We introduce dimensionless variables τ, x, y, and z defined by $q_{xx} = xS_0\eta_0/\Gamma$, $q_{xy} = yS_0\eta_0/\Gamma$, $q = zS_0\eta_0/\Gamma$, and $t = \tau/\omega$. In these variables, Eqs. (17)–(19) become

$$f^{-1}\dot{x} = [\exp(-\Delta\tau)\cos\tau]\left[\frac{2}{3}y + \frac{xy}{z}\right] - \frac{c}{\mu}xz , \qquad (20)$$

$$f^{-1}\dot{y} = [\exp(-\Delta\tau)\cos\tau]\left[-x - \tfrac{1}{3}z + \frac{y^2}{z}\right] - \frac{c}{\mu}yz , \quad (21)$$

$$f^{-1}\dot{z} = -[\exp(-\Delta\tau)\cos\tau]y - cz^2 , \qquad (22)$$

where $f = S_0/\omega$, $\mu = c/(c+k)$, and the dot indicates $d/d\tau$. Note that since no fluid-dependent quantities appear in the equations, they are, in particular, independent of the quench depth. However, the fluid properties and the quench depth enter the problem through the initial values of x, y, and z, which one must specify in order to determine a unique solution to Eqs. (20)–(22). We put $x(0) = y(0) = 0$ and $z(0) = z_0 = q_0\Gamma/\eta_0S_0$. This choice describes an interface with interfacial area per unit volume q_0 oriented isotropically at the initial time $t = 0$. We identify $t = 0$ with the moment of the quench and therefore ignore the time interval $0 < t < t_{cr}$ of early-stage spinodal decomposition. Here t_{cr} is the crossover time marking the beginning of the regime of capillary-driven domain growth; the subscript stands for crossover. Equations (20)–(22) are not applicable for times $t < t_{cr}$ since their phenomenological terms express the capillary-driven growth mechanism. Moreover, at sufficiently early times, the domains are presumably too diffuse for the interface tensor $q_{\alpha\beta}$ to be meaningful. However, we shall show that t_{cr} may be considered short compared with the times over which we perform the experiments, so that we may neglect the early stage of spinodal decomposition. We treat the initial interfacial area per unit volume q_0 as a free parameter, but we fix its dependence on the quench depth Q. Thus, light-scattering experiments on quiescent critical mixtures show that the characteristic domain size $a(t)$ at the time of the onset of linear growth t_{cr} is given by $a(t_{cr}) = b'\xi$, where ξ is the correlation length of equilibrium concentration fluctuations and b' is a constant of the order 10 [5,7,43]. We therefore write $q_0 \equiv 1/b\xi$, where b is of the same order as b'. The initial value of the scaled quantity z is then $z_0 = q_0\Gamma/\eta_0S_0$. A final form for this last expression results when we identify η_0 with the measured viscosity of the one-phase region $A\epsilon^{-0.040}$ and use the expressions $\xi = \xi_0\epsilon^{-0.63}$ and $\Gamma = \Gamma_0\epsilon^{1.26}$ to give $z_0 = B\epsilon^{1.93}$, where $\epsilon = Q/T_c^0$ and where $B = \Gamma_0/A\xi_0S_0b$ is treated as a free parameter.

We use a standard routine based on the Runge-Kutta

algorithm to solve Eqs. (20)–(22) numerically [44]. The computation yields the quantities x, y, and z as functions of the scaled time τ. As might be expected, $y(\tau)$ proves to be a function that oscillates about zero with a decaying amplitude and a phase that varies smoothly with respect to the phase of the oscillating shear rate. Writing the predicted shear component of the interfacial stress $\sigma_{xy}(t) = -\Gamma q_{xy}(t) = -S_0\eta_0y(\tau = \omega t)$ in the form of Eq. (11), we obtain

$$-y(\tau) = \exp(-\Delta\tau)[(\eta'/\eta_0)\cos(\tau) + (\eta''/\eta_0)\sin(\tau)] , \qquad (23)$$

where η' and η'' are here the real and imaginary parts of the predicted interfacial complex viscosity. In general, η' and η'' must depend on time if the calculated $y(\tau)$ is to be represented exactly by Eq. (23). During a single shear-rate oscillation, however, we expect that Eq. (23) holds as a good approximation with constant values for η' and η''. Equation (23) indicates that, in this case, (η'/η_0) and (η''/η_0) are given by the first two coefficients in a Fourier series expansion of $-y(\tau)\exp(+\Delta\tau)$ over the interval of scaled time of duration 2π. The values so obtained may be referred to the time that locates the middle of the interval. Thus we obtain the theoretical interfacial complex viscosity at the time $t = mT/2$ as

$$\frac{\eta'(t = mT/2)}{\eta_0} = \frac{1}{\pi}\int_{(m-1)\pi}^{(m+1)\pi}e^{\Delta\tau}[-y(\tau)]\cos\tau \, d\tau \equiv C_m , \qquad (24)$$

$$\frac{\eta''(t = mT/2)}{\eta_0} = \frac{1}{\pi}\int_{(m-1)\pi}^{(m+1)\pi}e^{\Delta\tau}[-y(\tau)]\sin\tau \, d\tau \equiv S_m , \qquad (25)$$

where $m = 1, 2, \ldots$ and $T = 2\pi/\omega$ is the oscillation period. By applying Eqs. (14), we can rewrite these expressions in terms of the interfacial viscosity $\Delta\eta$ and elastic shear modulus G:

$$\Delta\eta(t = mT/2)/\eta_0 = C_m + \Delta S_m , \qquad (26)$$

$$G(t = mT/2)/\eta_0\omega = (1 + \Delta^2)S_m . \qquad (27)$$

These may be compared to the measured quantities $(\eta - \eta_0)/\eta_0$ and $G/\eta_0\omega$ which are referred to the same times $t = mT/2$. Note that Δ is the damping in the right sides of Eqs. (26) and (27), but $\Delta\eta$ is the symbol for the interfacial viscosity.

It is to be noted that the computation of the reduced theoretical interfacial viscosity and elasticity modulus $\Delta\eta/\eta_0$ and $G/\eta_0\omega$ has been carried out without specifying any information that is specific to the fluid. The only inputs to the computation are the values of the parameters c, $\mu = c/(c+k)$, and the coefficient B which fixes the initial value $z_0 = B(Q/T_c^0)^{1.93}$ of the scaled interfacial area per unit volume in terms of the quench depth Q. We treat c, μ, and B as adjustable parameters. As discussed above, the value of η_0, which is needed only to reduce the experimental quantities, is taken directly from the data as the value at which the measured viscosity becomes constant after several oscillations.

A comparison of the theory and the experiment is shown in Fig. 6. The data are the same as shown in Fig. 5 but are now in reduced form. The values chosen for the adjustable parameters are

$$c = 0.038, \quad \mu = 0.8, \quad B = 7.6 \times 10^7 . \tag{28}$$

In choosing this set, we have favored the elastic shear modulus and obtained good agreement between theory and experiment for this property. The agreement between the measured and predicted interfacial viscosity is only qualitative. However, the theory reproduces the important features of the observed viscous behavior, such as the rapid decay to zero and the markedly high value just after the deepest quench. (That the measured $\Delta\eta$ decays to zero, not to any other constant value, has been arranged by our choice of η_0, while the behavior $\Delta\eta \rightarrow 0$ of the calculated $\Delta\eta$ is a nontrivial prediction of the theory.) From the value of the fitting parameter B, the relation $B = \Gamma_0/A\xi_0 S_0 b$ derived above, and the property amplitudes given in Table I, we find $b = 27$, where $q_0 = 1/b\xi$ is the initial value of the interfacial area per unit volume. Consistent with our neglect of the regime of early-stage spinodal decomposition, we identify q_0 with the interfacial area per unit volume at the time of the onset of the regime of capillary-driven domain growth.

It is interesting to compare these results with some related information recently obtained by Kubota *et al.* from light-scattering experiments performed on a sample at rest macroscopically [43]. These authors, who also worked with a critical IBA-plus-water mixture, determined the time of the crossover to the regime of linear domain growth t_{cr} to be $t_{cr} \approx 100(\xi^2/D)$. For times $t > t_{cr}$, the wave number k_m at which the intensity of the scattered light is maximum is given by $k_m = 16.9\xi/Dt$. Here ξ and D are the correlation length and mass diffusivity, respectively, in the one-phase region at the temperature $T > T_c$ such that $T - T_c = Q$, where Q is the quench depth. To analyze these findings, we assume that the mass diffusivity D satisfies the Stokes-Einstein relation $D = k_B T/6\pi\eta\xi$ [45] with the viscosity $\eta \equiv \eta_0 \equiv A(Q/T_c^0)^{-0.040}$ identified with η_0 and with the measured viscosity in the one-phase region, that the interfacial tension satisfies the two-scale-factor universality relation $\Gamma = k_B T/2.6\xi^2$ [36], and that the wave number of maximum scattering is related to the characteristic domain diameter $a(t)$ by $k_m(t) = 2\pi/a(t)$. With these assumptions and with $\xi = \xi_0(Q/T_c^0)^{-0.63}$ with $\xi_0 = 0.362$ nm [31], we calculate the crossover time t_{cr} as 15, 5, and 0.5 s for our quenches of depths 11, 19, and 64 mK. Thus, except during the earliest times of our shallowest quench, the regime of early-stage spinodal decomposition $t < t_{cr}$ takes place within about one shear-rate oscillation. The light-scattering experiment gives $a(t) = c'(\Gamma/\eta)t$, with $c' = 0.051$, for times $t > t_{cr}$. At the time t_{cr} of the onset of the regime of capillary-driven domain growth, the characteristic domain diameter is $a(t_{cr}) = b'\xi$ with $b' = 37$.

The numbers c' and b' are comparable with our c and b. We do not expect to find $c = c'$ and $b = b'$, because the inverse of the interfacial area per unit volume q^{-1} and the characteristic domain diameter a are not identical, but only of the same magnitude. We assume that $a(t)q(t) = F$, where F is a dimensionless constant of the order 1. We then have $c'/c = b'/b = F$. The constant F may be interpreted as the interfacial area per domain expressed in length units equal to the characteristic domain diameter. The value of F depends on the morphology of the concentration domains. For example, $F = 3$ for a regular array of cubes. A smaller value would be expected for a system of highly elongated, tubelike domains with smooth walls. Structure of this type has been observed in light-scattering studies of phase-separating mixtures subjected to steady shear [11,14]. From our experiment and analysis of the work reported in Ref. [43] we obtain $c'/c = 1.34$ and $b'/b = 1.37$. The two ratios are consistent, but seem too small to be the true value of F. There is, however, considerable uncertainty in the identification $k_m(t) = 2\pi/a(t)$. For example, Chou and Goldburg measured domain formation in a quenched critical mixture by light scattering and direct observation with a microscope and found that $a(t)k_m(t)$ ranges from 5 to 10 [5].

B. Stationary states and nonlinear viscoelasticity in the theory of Doi and Ohta

In our experiment, the amplitude of the oscillating shear rate decays in time. Consequently, the time-dependent behavior of the measured rheological properties is partly due to possible nonlinear effects (i.e., the dependence of the interfacial viscosity and elastic shear modulus on the shear-rate amplitude), as well as the explicit time dependence of the interface caused by its evolution as the phase separation proceeds. We can evaluate the contribution of the changing shear-rate amplitude by calculating the rheological properties as functions of time in the case that the applied oscillating shear rate has a constant amplitude and comparing the results with the previous computations in which the damping was included. Figure 7 shows the reduced interfacial viscosity $\Delta\eta/\eta_0$ and elastic shear modulus $G/\eta_0\omega$ calculated from the theory in the cases of damped and undamped oscillatory shear flows. The quench depth is 64 mK, and the solid curves, for which the damping $\Delta = 0.022$, are the same as the ones that appear in Fig. 6 for this quench depth. The dashed curves have been calculated with a constant shear-rate amplitude $S_0 = 7.9$ s^{-1} equal to the initial value of the shear-rate amplitude in the case that the damping is included. The curves suggest that the measured time-dependent behavior of $\Delta\eta$ and G during the latter half of the experiments in large part enters through their dependence on the shear-rate amplitude as the latter changes in time.

To investigate these effects more systematically, we consider the behavior of the solutions of Eqs. (20)–(22) at long times in the case $\Delta = 0$, i.e., when the shear rate oscillates in time with constant amplitude. We are concerned with the question of whether the solutions tend toward constant-amplitude, oscillatory functions of time. In the case that this is so, the interfacial viscosity $\Delta\eta$ and elastic shear modulus G become independent of time.
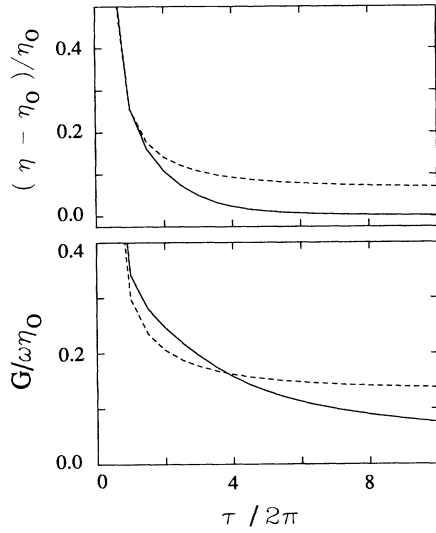
FIG. 7. Comparison of the rheological properties predicted by the theory in the case of damped and undamped oscillatory shear. The quench depth is 64 mK. The solid curves are the same as the ones appearing in Fig. 6 and show the effects of a damped oscillating shear rate $S(t) = S_0 \exp(-\Delta \omega t) \cos(\omega t)$ with $S_0 = 7.9$ s^{-1}, $\Delta = 0.022$, and $\omega = 1.58$ Hz. The dashed curves show the effects of a shear rate that oscillates with constant amplitude so that $S(t) = S_0 \cos(\omega t)$ with $S_0 = 7.9$ s^{-1}.

Their dependence on the shear-rate amplitude S_0 and the frequency ω can then be investigated without the necessity of treating the system's evolution in time. We are not able to establish analytically the existence of periodic solutions of Eqs. (20)–(22), but again rely on numerical methods. Specifically, starting from the initial conditions $x(0) = y(0) = 0$ and $z(0) = z_0 = 0.60$, we have solved Eqs. (20)–(22) (with $\Delta = 0$) over the time range $0 \leq \tau \leq 60\pi$ (i.e., 30 shear-rate oscillations.) The value $z_0 = 0.60$ corresponds to a quench of depth 19 mK, but we have verified that the long-time behavior which concerns us here is independent of the value of z_0. The form of Eqs. (20)–(22) shows that the rheological character of the interface depends on the shear-rate amplitude S_0 and the frequency ω only through the ratio $f = S_0/\omega$. This unusual situation comes about because, as discussed by Doi and Ohta, the theory does not have an intrinsic time scale [20]. Whereas in the previous computations we have used for f the value $f = 5$, which is the ratio $S_0/\omega = 7.9$ s$^{-1}/1.58$ Hz $= 5.0$ of the values appropriate to the experiment, in the present context we consider the behavior of the solutions as f is varied over a wide range. To address the question of whether the solutions tend to periodic functions, we analyze their behavior over the last ten shear-rate oscillations (i.e., cycles 20–30.) The results indicate that there is a critical value f_c for f such that the solutions of Eqs. (20)–(22) tend toward oscillations with constant amplitudes when $f > f_c$. That is, for large values of f the shear distortion is effective enough and the domain growth can be stopped, resulting in dynamical equilibrium of the domain size distribution.

When $f < f_c$, the amplitudes decay indefinitely. Thus for small values of f the effect of the shear becomes weak and the domain growth cannot be stopped, leading to macroscopic phase separation. The value of f_c depends only on the parameter μ [46]. We have studied most extensively the case $\mu = 0.8$, for which $f_c \approx 5$. We find that, with $f \geq 5.4$, the fractional change per cycle of the amplitude of the function $y(\tau)$ (which is the scaled interfacial shear stress) over cycles 20–30 is of the order 10^{-6} and may have either sign. Since nonconstancy of the amplitudes at this level may be attributed to the accuracy of the algorithm, we conclude that Eqs. (20)–(22) do in fact attract periodic solutions for $\Delta = 0$ and $f > f_c$ [47]. On the other hand, over the same range of times (20–30 shear-rate cycles) and with $3 \leq f \leq 4.4$, our computations show that the amplitude of $y(\tau)$ decays with a fractional change per cycle of the order 10^{-2}. The decay is very slow, however, and in fact appears to be like τ^{-1}. In our actual experiments, where f is effectively ramped downwards through a range of values of f less than f_c, we see a combination of this slow decay and a stronger decay, best thought of as an implicit time dependence due to the changing f.

Figure 8 shows a plot of the interfacial viscosity $\Delta \eta$ and the elastic shear modulus G, resulting at long times when the interface is subjected to an oscillating shear flow, as predicted from the theory of Doi and Ohta. The value of the phenomenological parameter μ is 0.8 [46]. The properties have been reduced by a new quantity η_∞ defined by

$$\eta_\infty = \frac{\mu(1-\mu)}{3c(1+\mu)^2} \eta_0 , \qquad (29)$$

which is the interfacial viscosity that results at long times when the interface is subjected to a constant (nonoscillatory) shear flow, according to the theory. This result is
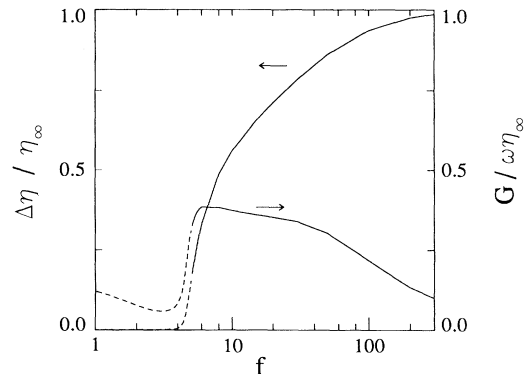

FIG. 8. Reduced interfacial viscosity $\Delta \eta/\eta_\infty$ and reduced elastic shear modulus $G/\omega \eta_\infty$ predicted by the theory for constant-amplitude oscillatory shear as functions of $f = S_0/\omega$. The properties have been reduced by the steady-state interfacial viscosity $\eta_\infty = \mu(1-\mu)\eta_0/3c(1+\mu)^2$ predicted by the theory in the case of a constant (nonoscillatory) shear flow. See the text for the meaning of the dashed sections of the curves.

readily found from Eqs. (20)–(22) by replacing [exp($-\Delta\tau$)cosτ] by 1, as is appropriate for a steady shear, setting $\dot{x}=\dot{y}=\dot{z}=0$, solving for x, y and z the system of algebraic equations that results, and thus obtaining a constant solution to the system of differential equations. We have established numerically that all time-dependent solutions approach this constant solution at long times. Figure 8 shows that the steady-state interfacial viscosity under an oscillating shear flow is shear thickening and frequency thinning since it increases with the ratio $f=S_0/\omega$. In contrast, the interfacial viscosity under a constant shear flow is Newtonian at long times, since its value η_∞ does not depend on the shear rate [see Eq. (29)]. As $f\to\infty$, the rheological response of the interface under an oscillating shear flow becomes purely viscous with a viscosity that approaches η_∞, but the convergence is very slow. As has been discussed, the computations indicate that periodic solutions to Eqs. (20)–(22) such that the rheological properties are independent of time are obtained only in the case that $f>f_c$, where $f_c\approx5$ for $\mu=0.8$. Figure 8 shows that both the interfacial viscosity and the shear modulus are strongly shear dependent in the vicinity of $f=5$. When $f<f_c$, the properties never become independent of time but decay indefinitely. The sections of the curves for which $f<5$ have accordingly been drawn with broken lines, since here steady-state solutions do not exist. These sections merely represent the calculated rheological behavior at a particular time, namely the twentieth oscillation cycle. The qualitative behavior shown by these sections of the curves is relevant to the experiment, however. They indicate that, at sufficiently low f, the rheological behavior of the interface may be entirely elastic, although also time dependent, as illustrated in Fig. 8, showing that for $f<4$ there is a region where the viscous enhancement is negligible, while the elasticity of the fluid is appreciable. This situation will not last: G will go to zero as time goes on and Fig. 8 only indicates the conditions at a particular time. However, the decay is slow, and for a wide range of times we expect a purely elastic response from the interface, as was actually seen in the experiment (Fig. 6), where the decay of the disk's motion effectively ramps the value of f through the range $1.2\leq f\leq5$.

IV. OFF-CRITICAL MIXTURES

Figures 9 and 10 show the viscosity and elastic shear modulus as functions of time as measured during quenches in an IBA-rich mixture, $X=0.426$, and a water-rich mixture, $X=0.343$. Here X denotes the IBA mass fraction. These two off-critical mixtures differ remarkably from the critical mixture and from each other in their rheological behavior during phase separation. Both mixtures show large viscosity enhancements which remain essentially constant during the measurements and increase with the quench depth. Elasticity is present in the case of the IBA-rich mixture (Fig. 9), with the elastic modulus G increasing with time. The initial values of G are *negative* for deep quenches. During the latter half of the measurements, G is positive for quenches of all depths, varies less rapidly, and increases with quench
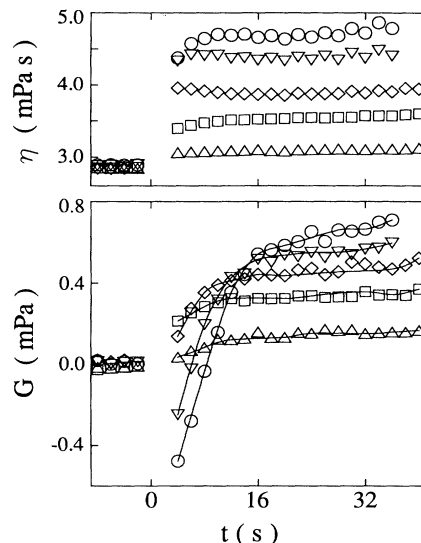

FIG. 9. Viscosity η and elastic shear modulus G as functions of time during the phase separation of an IBA-rich mixture. The curves shown for G are guides to the eye. $\bigcirc$, 172 mK; $\triangledown$, 95 mK; $\diamondsuit$, 37 mK; $\square$, 23 mK; $\triangle$, 9 mK.

depth. In striking contrast, elasticity is absent in the case of the water-rich mixture (Fig. 10): the values of G after the quench are distributed about zero with about the same level of scatter that we see before the quench, while the mixture is in the one-phase region.

In the remainder of this section, we shall develop some ideas toward understanding the observed behavior of these mixtures. We show that the quench-depth dependence of the viscosities, and also the order of magnitude of their values, can be predicted from constitutive equations which have been proposed to describe dilute emulsions. These theories also predict a positive elastic shear modulus that increases with the volume fraction and the radius of the droplets of the suspended phase. Drawing
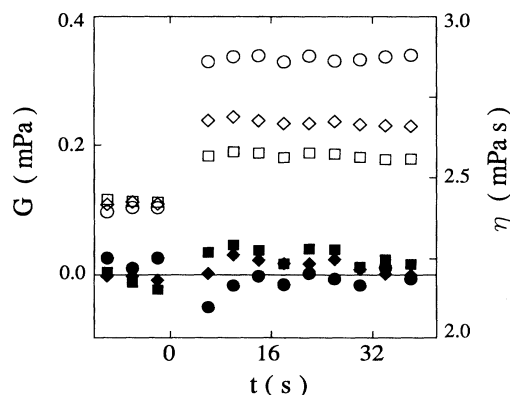

FIG. 10. Viscosity η (open symbols) and elastic shear modulus G (closed symbols) as functions of time during the phase separation of a water-rich mixture. $\bigcirc$ and $\bullet$, 241 mK; $\diamondsuit$ and $\blacklozenge$, 80 mK; $\square$ and $\blacksquare$, 40 mK.

from other experimental and theoretical studies on concentration-cluster size and growth in quenched off-critical liquid mixtures, we can explain why the elasticity of the IBA-rich mixture in phase separation increases with time and also predict its order of magnitude during the latter half of our measurements when its value is positive. We cannot explain the details of its time and quench-depth dependence or its initially negative value, nor do we understand the absence of elasticity during the phase separation of our water-rich mixture.

In a classic paper, Taylor has calculated the effective viscosity of a dilute emulsion consisting of spherical droplets of a liquid with viscosity η_d (droplet viscosity) suspended in a liquid with viscosity η_s (suspending-liquid viscosity) [48]. We denote Taylor's result by η_T:

$$\eta_T = \eta_s(1 + \tfrac{7}{4}f_1\phi) , \qquad (30)$$

with

$$f_1 = \frac{10\lambda + 4}{7(\lambda + 1)} , \qquad (31)$$

where $\phi \ll 1$ is the volume fraction of the droplets and $\lambda = \eta_d/\eta_s$ is the ratio of the viscosities of the liquids. For equal viscosities, $f_1 = 1$. The restriction to low volume fraction allows hydrodynamic interactions between the droplets to be neglected. The stipulation that the droplets remain spherical under shearing of the emulsion is satisfied for sufficiently low values of the capillary number Ca, defined as

$$\mathrm{Ca} = \frac{R\eta_s S}{\Gamma} , \qquad (32)$$

where R is the droplet radius, S is the shear rate, and Γ is the interfacial tension [48,49]. Taylor's theory applies in the case where the shear flow is steady. Oldroyd has generalized the theory to include weakly time-dependent flows [50]. His treatment yields the constitutive equation of a dilute emulsion in the form of an equation relating the stress and strain-rate tensors $\sigma_{\alpha\beta}$ and $D_{\alpha\beta}$ and their time derivatives:

$$\left[1 + \lambda_1 \frac{d}{dt}\right]\sigma_{\alpha\beta} = 2\eta_T\left[1 + \lambda_2 \frac{d}{dt}\right]D_{\alpha\beta} . \qquad (33)$$

Here, λ_1 and λ_2 are the so-called relaxation and retardation times defined by

$$\lambda_1 = \lambda_0\left[1 + \frac{1}{5}\frac{19\lambda + 16}{(\lambda + 1)(2\lambda + 3)}\phi\right] , \qquad (34)$$

$$\lambda_2 = \lambda_0\left[1 - \frac{3}{10}\frac{19\lambda + 16}{(\lambda + 1)(2\lambda + 3)}\phi\right] , \qquad (35)$$

$$\lambda_0 = \frac{(19\lambda + 16)(2\lambda + 3)}{40(\lambda + 1)}\frac{\eta_s R}{\Gamma} , \qquad (36)$$

while the strain-rate tensor $D_{\alpha\beta} = \tfrac{1}{2}(\partial v_\alpha/\partial x_\beta + \partial v_\beta/\partial x_\alpha)$ is calculated from the macroscopic fluid velocity v. In the case where v has the form of the Couette flow given by Eq. (9) and the shear rate $S(t)$ oscillates sinusoidally with frequency ω, Eq. (33) yields the shear-stress component σ_{xy} in the form of Eq. (13) with the effective viscosity η and elastic shear modulus G of the emulsion

given by

$$\eta = \eta_T\frac{1 + \lambda_1\lambda_2\omega^2}{1 + (\lambda_1\omega)^2} \to \eta_T , \qquad (37)$$

$$G = \eta_T\omega^2\frac{\lambda_1 - \lambda_2}{1 + (\lambda_1\omega)^2} \to \frac{245}{64}f_2\phi\omega^2\eta_s^2 R/\Gamma . \qquad (38)$$

Here, $f_2 = [2(19\lambda + 16)/35(\lambda + 1)]^2$ with $\lambda = \eta_d/\eta_s$; $f_2 = 1$ in the case of equal droplet and suspending-liquid viscosities η_d and η_s. The limits indicated here give the behavior at low frequencies $\omega\lambda_0 \ll 1$. This limit holds in all of our experiments.

In order to compare the measured rheological properties of the mixtures undergoing the time-dependent process of phase separation with the theoretical properties of emulsions, in principle we must regard all of the quantities ϕ, η_s, η_d, Γ, and R as time dependent. As a practical alternative, suggested by the observed time independence of the viscosity, we instead take the droplet radius R to be the only changing quantity and identify ϕ, η_s, η_d, and Γ with their values in the equilibrium, two-phase state. These can be calculated from determinations of the properties of the equilibrium states reported in the literature. The expressions we use for the properties of the coexisting phases are given in Table I. In particular, the volume fraction in equilibrium of the minority phase, which we identify with the volume fraction of the suspended droplets of the emulsion, may be calculated approximately from [7]

$$\phi \approx \frac{1}{2}\left[1 - \left[\frac{\Delta T}{\Delta T + Q}\right]^\beta\right] , \qquad (39)$$

where $\beta = 0.324$ is the coexistence-curve exponent, $\Delta T = T_c - T_{cx}$ is a function of the composition X of the off-critical mixture, and $Q = T_{cx} - T_f$ is the quench depth, T_f being the equivalent final temperature after a pressure quench. From the information for the coexistence curve given in Table I, we calculate $\Delta T = 32$ mK for the IBA-rich mixture and $\Delta T = 61$ mK for the water-rich mixture. In calculating ϕ, we make small corrections to Eq. (39) to take into account the density difference of the phases and the asymmetry of the coexistence curve [32,34,35]. These corrections amount to 5% at most. The form of the expression we use to calculate the viscosities of the coexisting phases as functions of the quench depth was suggested by a figure in Ref. [32]; we have evaluated the two parameters from an analysis of the viscosity data given in Ref. [37].

We are left with the specification of the droplet radius R, which we identify with the characteristic radius of clusters of the new phase and which will contain all the time dependence of the phase-separation process in our simplistic treatment. Homogeneous and heterogeneous nucleation, as well as spinodal decomposition, are all possible mechanisms for the decay of supersaturated, one-phase mixture states. Here for simplicity we develop a picture based on homogeneous nucleation. In homogeneous nucleation, thermal fluctuations are the origin of microscopic clusters larger than the critical size $R_c \approx \xi^-/3\phi$

for stability against reevaporation of the cluster back into the supersaturated, continuous phase [1,3]. Here, ξ^- is the correlation length of concentration fluctuations in the coexisting phases. Such microscopic clusters are produced at an appreciable rate in quenches at least as deep as the cloud point given by the classical Becker-Döring theory as $0.15\Delta T$ [1]. All the quenches we report here are at least this deep. Clusters larger than the critical size can grow to mesoscopic size in several different ways that have been observed in experiments or considered in theories. For orientation, we compare five cluster-growth mechanisms in Table II. In addition to the expressions for the cluster radius as a function of time, the table gives the numerical value of the cluster radius at time $t = 30$ s in the case of our typical quench of depth 94 mK performed on the IBA-rich mixture. Lifshitz-Slyozov condensation and Brownian coalescence of clusters have been studied theoretically by Siggia [4] and experimentally by Wong and Knobler [7]. Both mechanisms predict the growth of clusters according to $t^{1/3}$ during a late-stage regime when the presence of a cluster has established a depletion of either the supersaturation of the continuous phase or the number density of other clusters in the cluster's vicinity. Recent works of Cumming et al. [51] and Baumberger, Perrot, and Beysens [13] establish the relevance to experiments of an earlier, "free-growth" regime, where condensation occurs at essentially fixed supersaturation of the continuous phase. Of the most relevance to our problem are two mechanisms that involve shear flow. Baumberger, Perrot, and Beysens also studied phase separation under steady shear of a water-rich mixture of IBA and water with a composition very close to that of our own mixture [13]. They find growth of the clusters according to a power of St close to 0.685, where S is the shear rate. From the equations that describe the transport of material to the clusters under the

combined action of mass diffusion and advection in the shear flow of the continuous phase, they derive a scaling relation for R and t in terms of D^-, S, and ϕ that collapses their data taken in quenches of various depths and at various shear rates. Here D^- is the mass diffusivity in the two-phase region. This advection-diffusion mechanism is also expected to be effective during an early stage where the decrease of the supersaturation of the continuous phase may be small. The last cluster-growth mechanism we consider, shear-induced coalescence and burst, is expected to dominate in the opposite limit, when the volume fraction of the new phase actually present has nearly attained its equilibrium value ϕ and the supersaturation of the continuous phase is therefore nearly zero. Onuki has argued that, because of the relative motions which the clusters undergo as a result of the gradients in the fluid velocity, collisions of clusters are greatly enhanced and produce extremely rapid cluster growth by coalescence according to $R(t) \sim \exp(\phi St)$ [10]. In this way the clusters can quickly attain the radius $R_{\text{burst}} = Ca_c \Gamma / \eta_s S$, whereupon they are ruptured by the viscous forces of the shear flow [10,49]. Here, Ca_c is the critical value of the capillary number, which is a function of the tensorial character of the flow and the ratio λ of the viscosities of the liquids forming the droplet and the continuous phase. Its value is 0.35 for the case of equal viscosities and a Couette flow [49]. A stationary distribution of cluster sizes narrowly peaked near R_{burst} is predicted to result in this process. Although some aspects of the theory of Onuki may be questionable [52], quantitative experimental confirmations of the picture described above have been provided by a number of experiments on stationary-process nucleation in supercooled binary liquid mixtures under shear [12].

In calculating values of the cluster radius $R(t)$ from the two shear-dependent cluster-growth laws, we have set the shear rate S to a constant value of 5 s^{-1}. This value represents the typical amplitude of the shear rate near the middle of our quench experiments on the IBA-rich mixture, but our shear rate also oscillates. The oscillation may certainly have a significant effect on the advection-diffusion or shear-induced coalescence processes, but we have not attempted to estimate the effect. We similarly calculate R_{burst} using $S = 5$ s^{-1}, although it is known that droplet burst is affected by the history of the flow in the case where the flow is time dependent. The value of Ca_c given above applies to a steady flow at a shear rate which has been increased quasistatically [49].

In Figs. 11 and 12, we compare the viscosity and elastic shear modulus of the two phase-separating, off-critical mixtures with the predicted properties of dilute emulsions. The viscosity-enhancement ratio $(\bar{\eta} - \eta_s)/\eta_s$ and the elastic modulus $\bar{G}$ are plotted as functions of the volume fraction ϕ. Here, $\bar{\eta}$ and $\bar{G}$ are time averages of the values of η and G measured during the latter part of the quench experiments 22 s $\leq t \leq$ 36 s when the time dependence of the properties is weak. The viscosity η_s of the majority phase in its equilibrium state is calculated from the expressions appearing in Table I. The measured viscous enhancement ratio $(\bar{\eta} - \eta_s)/\eta_s$ is compared with the Taylor expression $7 f_1 \phi / 4$ [see Eq. (30)] which does

TABLE II. Mechanisms of cluster growth in phase-separating off-critical mixtures.

Mechanism	Cluster radius	Typical value[a]
Lifshitz-Slyozov condensation[b]	$R = (0.053 D^- \xi^- t)^{1/3}$	0.5 μm
Free growth[c,d]	$R = (2\phi D^- t)^{1/2}$	6.0
Brownian droplet coalescence[b]	$R = (12\phi \frac{6}{5} D^- \xi^- t)^{1/3}$	1.8
Advection-diffusion in a shear flow[c]	$R = 1.08(D^- / S)^{1/2}(2\phi St)^{0.685}$	13.6
Shear-induced droplet coalescence and breakup[e]	$R \propto \exp(\phi St) \rightarrow R_{\text{burst}} = Ca_c \Gamma / \eta_s S$	16.7

[a]At time $t = 30$ s following a quench of depth 94 mK performed on a mixture for which $T_c - T_{\text{cx}} = 32$ mK and which is sheared at a constant rate $S = 5$ s^{-1}.
[b]Reference [4].
[c]Reference [13].
[d]Reference [51].
[e]References [10], [12], and [49].

not contain the droplet radius R. Two curves computed from the low-frequency limit of the elasticity modulus given in Eq. (38) are shown for comparison with the measured values of $\bar{G}$. The solid curves have been calculated with the values of the droplet radius R prescribed by the advection-diffusion expression $R(t) = 1.08(D^-/S)^{1/2}(2\phi S t)^{0.685}$, with $S = 5$ s^{-1} and the time t set equal to $t = 30$ s. The dashed curve has been calculated with R set equal to $R_{\text{burst}} = 0.35\Gamma/\eta_s S$, as may result under the shear-induced coalescence and burst processes. The plots show that for both mixtures the measured viscosity enhancement $(\bar{\eta} - \eta_s)/\eta_s$ is approximately linear in the equilibrium minority-phase volume fraction ϕ. In the case of the water-rich mixture, the agreement between the measurements and Taylor's expression for the effective viscosity of an emulsion is good. The viscosity enhancements we measure for the IBA-rich mixture are about twice the theoretical ones, however. The experimental values of the time-averaged elastic shear modulus
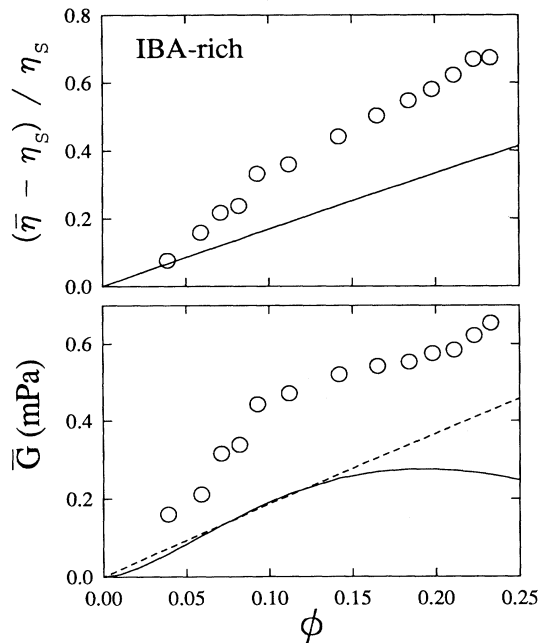

FIG. 12. Same treatment as that of Fig. 11 of results obtained on a water-rich mixture.

FIG. 11. Reduced interfacial viscosity $(\bar{\eta} - \eta_s)/\eta_s$ and elastic shear modulus $\bar{G}$ of a phase-separating IBA-rich mixture as functions of the volume fraction ϕ of the equilibrium minority phase in the two-phase state. The viscosity of the equilibrium majority phase is η_s. The quantities $\bar{\eta}$ and $\bar{G}$ are time averages over the interval 22 s $\leq t \leq 36$ s of the measured time-dependent values of the viscosity η and elastic modulus G. The curve shown in the plot of viscosity represents Taylor's expression for the viscosity of a dilute emulsion. The curves shown in the plot of the shear modulus have been calculated from Oldroyd's theory for a dilute emulsion. For the solid curve, we have set the droplet radius to the cluster radius calculated at the time $t = 30$ s under cluster growth by an advection-diffusion mechanism described in Ref. [13]. The dashed curve corresponds to a droplet radius equal to the maximum radius R_{burst} that a droplet may have without being burst by the shear flow.
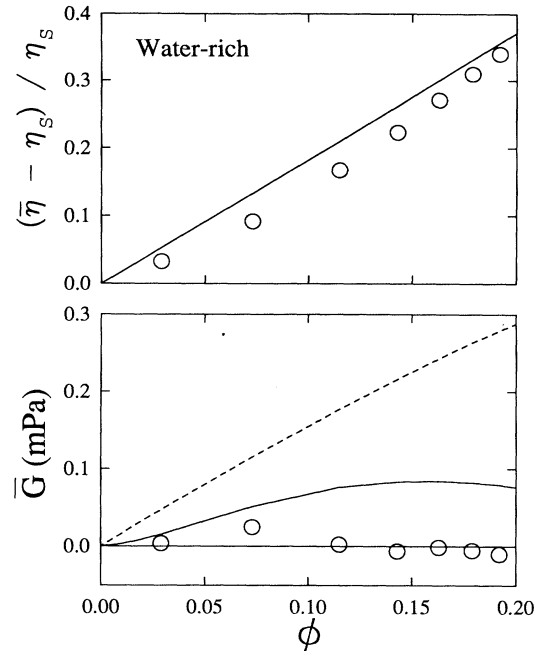
$\bar{G}$ for this mixture are also about two times larger than the calculated ones. The data are noisy, but there is a clear rounding-off trend at higher volume fractions. The shape bears some resemblance to that of the theoretical curve which we calculate with the droplet radius R prescribed by the formula that expresses growth by the advection-diffusion process. The rounding off occurs because, with this mechanism of growth, the quench-depth dependence of droplet growth is weaker than that of the interfacial tension Γ. In calculating the dashed curve we set $R = R_{\text{burst}} \propto \Gamma$; a nearly linear dependence of $\bar{G}$ on ϕ then results. The near coincidence over part of the range of ϕ of the two theoretical curves for $\bar{G}$ in Fig. 11 is fortuitous since the growth mechanisms are quite different, but it indicates that conditions during the experiments are such as to produce droplets whose sizes are of the order of R_{burst}, even if only by the comparatively slower advection-diffusion growth mechanism. Taking $R = R_{\text{burst}}$ we predict about the same values for $\bar{G}$ for the water-rich mixture as for the IBA-rich mixture, while, with R calculated from the advection-diffusion expression, we predict values for $\bar{G}$ smaller by a factor of about 3. However, the smaller theoretical values are still inconsistent with our observation of $\bar{G} = 0$ within a resolution of about 0.02 mPa for the water-rich mixture.

V. DISCUSSION AND CONCLUSIONS

We have measured the effective viscosity η and elastic shear modulus G of the critical and two off-critical mixtures of isobutyric acid (IBA) and water during the process of phase separation. Qualitatively different behavior was observed in each case. Quenches of the critical mixture produced rapidly decaying values of the viscosity

enhancement $\Delta\eta$ and the shear modulus G. We showed that this behavior is predicted by a phenomenological theory of the stress generated by a coarsening bicontinuous interface subjected to shear [20]. The theory allows us to attribute the observed rapid decay of $\Delta\eta$ and G to the rapid, capillary-driven decrease of the amount of interfacial surface in the system. By appropriately choosing three phenomenological parameters, we were able to obtain satisfactory agreement between the theory and the measurements. Two of the parameters are related to quantities that can be obtained in light-scattering experiments performed with mixtures undergoing phase separation while macroscopically at rest. We showed how information about the structure of domains could in principle be obtained from a comparison of these related parameters.

We found that the two off-critical mixtures, one of which was rich in water and the other rich in IBA, exhibited similar viscous behavior during phase separation. In contrast to the decreasing viscosities of the critical mixture, both off-critical mixtures produced viscosity enhancements essentially independent of time for times up to about 40 s, the duration of our quench measurements. The enhancements increased linearly with the volume fraction of the new phase, which is a function of the depth of the quench. The two mixtures were strikingly unlike in their elastic behavior, however, since the IBA-rich mixture produced values of G that increased as a function of time since the moment of the quench, while the water-rich mixture showed no elasticity at all, within the resolution of our measurement.

We find, then, that of the rheological behavior during phase separation of the critical and off-critical mixtures, it is the latter that has proved the more difficult to explain quantitatively. Although the domain morphology that results after a quench of the critical mixture is more complicated than with which results after a quench of an off-critical one, many details of the intricate configuration of the domains are integrated out in the construction of the interface tensor $q_{\alpha\beta}$, which governs the macroscopic stress. A phenomenological equation of motion for the evolution of $q_{\alpha\beta}$ has then proved adequate to predict the observed rheological behavior. On the other hand, the appearance of the new phase in the form of relatively isolated and compact clusters, as is presumably the case during the phase separation of off-critical mixtures, invites us to attempt a more detailed, microscopic level of description. But this has proved to be difficult. Our experiments show that the behavior of ideal emulsions, in which the rheological behavior is entirely due to the regions of higher shear rate that result from the fluid flow around and inside the spherical, noninteracting droplets, is at least relevant in order of magnitude to the behavior of off-critical mixtures undergoing phase separation under shear. However, refinement of this picture to the level of a quantitative theory will require significant advances in our understanding of several problems. Some of these are nucleation and cluster-growth dynamics in phase-separating liquid mixtures under shear flows, the deformation and burst of droplets in time-dependent shear flows, droplet coalescence, and the bulk behavior, via a

constitutive equation, of a suspension of droplets under conditions of high droplet deformation, burst, and coalescence. Each of these presents in its own right a formidable problem.

We conclude with some more speculative comments on the two puzzling results of the experiments on off-critical mixtures. These are the observation of a negative elastic shear modulus immediately following deep quenches of the IBA-rich mixture, and the strikingly unlike behavior with regard to elasticity of the IBA-rich and water-rich mixtures.

A negative elastic modulus describes a material that, under deformation, generates a stress that acts to increase the deformation. Now this situation can come about in theoretical models. For example, Khan and Armstrong have calculated the stress-strain curve of a concentrated two-dimensional foam consisting of hexagonal bubbles with rounded corners [53]. The slope of the curve becomes negative when the strain is made so large that a new equilibrium configuration is related to the original one by a sideways shift of a layer of bubbles by the interstitial spacing. A real material, however, reaches a yield point and flows and does not exhibit negative elasticity under a static strain. Our observation of $G < 0$ is sufficiently surprising that it is natural to return to our raw experimental observation and consider whether another interpretation might be more physical. Here, the raw observation is that during the first few oscillations of the disk that occur after deep quenches of the IBA-rich mixture, the period T is too large in comparison with the damping Δ in the sense that $T/T_0 > 1 + \Delta$, where $T/T_0 = 1 + \Delta$ is the consistency relation that yields $G = 0$ for a purely viscous fluid [54]. The consistency relation expresses the fact that the time-varying drag exerted by the fluid on the disk has two components of approximately equal magnitude, one in phase with the negative of the disk's angular velocity $-\dot{\alpha}(t)$, and the other in phase with the disk's angular position $\alpha(t)$. This second component acts in opposition to the restoring torque $-\kappa\alpha(t)$ supplied by the suspension wire with spring constant κ and results in the increase of the period with respect to the period in vacuo T_0. The existence of the second drag component is due to the fluid's inertia. In oscillating-body viscometry, it is in fact conventional to attribute the increase of the period to an increase of the disk's moment of inertia by that of a shell of fluid that moves with the disk as a rigid body. With this concept in mind, it is natural to try to account for the even further increase of the period during the early times of our deep-quench experiments on the IBA-rich mixture by assuming a further contribution of the fluid to the disk's moment of inertia, rather than by attributing negative elasticity to the fluid. The picture we have in mind here is of droplets of the new phase that stick to the disk and therefore increase the period by adding to the moment of inertia. However, simple estimates show that this effect is small. For example, the disk's oscillation period would be increased only by about 0.8 ms due to the added moment of inertia of a shell of fluid of thickness 10 μm moving rigidly with the disk. On the other hand, the initial value of the elastic shear modulus $G = -0.48$ mPa which we referred to time

$t = 4$ s after a quench of depth $Q = 172$ mK of the IBA-rich mixture (Fig. 11) corresponds to a value of the period longer by 6.7 ms than the value which would yield $G = 0$, given the same value of the damping Δ.

We have also estimated the modification to the drag exerted by the fluid on the oscillating disk in the case where a thin, smooth layer of fluid with viscosity η_d separates the disk from the bulk of the fluid whose viscosity has a complex value η^*. Such a layer is supposed to undergo a shearing motion rather than the rigid-body motion considered above and introduces small changes in the amplitude and phase of the oscillating drag which are of the order $L/|\delta^*|$, where L is the thickness of the layer and $|\delta^*| \approx 1$ mm is the boundary-layer thickness of the flow. Thus, a layer thickness much larger than a typical droplet size of $R \approx 10$ μm (see Table II) would have to be supposed to explain the initially negative value of G on the basis of either a sheared or rigidly moving layer. Moreover, we should have to suppose that the layer thickness decreased in time. We consider this situation to be unlikely, although we are aware of a recent experiment by Bodensohn and Goldburg in which thick wetting layers of decreasing thickness formed during the phase separation of a critical mixture confined between closely spaced plates [55]. Our own experiments with the critical IBA-plus-water mixture do not show evidence of this effect, which depends essentially on the confined geometry. During the phase separation of a critical mixture near a wall, but in an otherwise unconfined geometry, the thickness of the wetting layer is of the order of the characteristic size of domains in the bulk and increases, as has been observed in an experiment reported by Guenoun, Beysens, and Robert [56]. We are, therefore, persuaded that the negative values of the elastic shear modulus which we infer from the period and damping of the disk's motion truly describe the stress-strain relation of the bulk material. We speculate that the negative elasticity could come about during droplet coalescence or during the slipping of droplets past each other in a manner similar to the behavior of the model foam [53].

We turn finally to the unlike behavior of the two off-critical mixtures. Their mass fractions $X = 0.426$ and 0.343, respectively, for the IBA- and water-rich mixtures, differ from the critical composition $X_c = 0.388$ by roughly equal amounts. We would therefore expect the phase-separation processes in the two mixtures following quenches of similar depths to be similar. The typical magnitude, say $\bar{G} = 0.5$ mPa, of the elastic shear modulus at times near $t \approx 30$ s which we measure during the phase separation of the IBA-rich mixture implies through Eq. (38) a value of about 20 μm for the droplet radius R. A value of this order is consistent with what we predict for clusters of the new phase growing by the advection-diffusion process or maintained at the breakup radius R_{burst} by the shear-induced coalescence and burst process. Now we would expect these processes to be equally effective in the phase separation of the water-rich mixture. But the experimental result $\bar{G} = 0 \pm 0.02$ mPa sets through Eq. (38) a limit of about 3 μm for the droplet radius. Our experiments therefore suggest that the phase-separation process could be qualitatively different for mixtures symmetrically placed on opposite sides of the phase diagram.

An obvious alternative explanation is that the unlike rheological behavior of the two mixtures has to do with the differing tendencies of the new phase to wet the surface of the disk. In fact, the wetting properties of the suspended phase are known to have important effects on the measured behavior of emulsions. For example, Princen measured the viscosity and static-shear elasticity modulus of concentrated oil-in-water emulsions using a rotating-cylinder rheometer [57]. He found that the behavior was erratic in the case that the rheometer's concentric cylinders were made of a hydrophobic material (stainless steel) which was wet by the oil droplets. Reproducible results were obtained with cylinders made of a hydrophilic material (pyrex). Then, however, important corrections had to be made for a slipping effect in which a large part of the decrease of the fluid velocity between the rotating and stationary cylinders occurred in thin, watery layers at the cylinder surfaces. Now the disk of our viscometer is made of Hastelloy C-276, which is wet by IBA and not wet by water. Therefore, if analogous wetting effects occur in our system, slipping should be expected during the phase separation of the IBA-rich mixture, when the disk's surface may repel the water-rich clusters. But in fact it is with this mixture that we see the elasticity and the stronger viscosity enhancements, and this behavior does not suggest slipping. On the other hand, during the phase separation of the water-rich mixture, a smooth layer of the new, IBA-rich phase with a thickness comparable to the radius of the clusters occurring in the bulk may form on the surface of the disk. As we have mentioned, a thin, smooth layer has a small effect on the drag which the fluid exerts on the disk. These considerations lead us to suspect that the unlike behavior of the two off-critical mixtures is not caused by wetting effects, but rather to some aspect of cluster growth, burst, or coalescence in the bulk of the samples that is dissimilar in quenches of the same depth performed on mixtures whose compositions are symmetrically located about the critical composition.

ACKNOWLEDGMENTS

APPENDIX

Because the unknown η^* appears in Eq. (8) in the form $\delta^* = (\eta^*/\rho\omega_0)^{1/2}$, we introduce unknowns u and w defined by $(\eta^*)^{1/2} = u + iw$. According to standard usage in oscillating-body viscometry, we write $\Theta = T_0/T$ for the ratio of the period *in vacuo* to the period measured with the fluid present, and we write the required powers of the measured complex number $s = (-\Delta + i)\Theta$ as $s^{1/2} = x + iy$

and $s^{3/2}=-H_2+iH_1$ [41]. Some manipulation of Eq. (8) then yields

$$2\Delta\Theta^2=k_1(H_1u-H_2w)-k_2\Theta(u^2-w^2-2\Delta uw)$$
$$-k_3[y(u^3-3uw^2)+x(3u^2w-w^3)]\,,\qquad(A1)$$

$$1-\Theta^2+(\Delta\Theta)^2=k_1(H_2u+H_1w)$$
$$-k_2\Theta[\Delta(u^2-w^2)+2uw]$$
$$+k_3[x(u^3-3uw^2)-y(3u^2w-w^3)]\,,$$
$$\qquad(A2)$$

where

$$x=\left[\frac{\Theta}{2}[(\Delta^2+1)^2-\Delta]\right]^{1/2}\,,\qquad(A3)$$

$$y=\frac{\Theta}{2x}\,,\qquad(A4)$$

$$H_1=3\Theta x/2-\left[\frac{\Theta}{2x}\right]^3\,,\qquad(A5)$$

$$H_2=3\Theta^2/4x-x^3\,,\qquad(A6)$$

$$k_1=\left[1+4\frac{h}{R_d}\right]\frac{\rho R_d}{\bar{\rho}h}\chi\,,\qquad(A7)$$

$$k_2=B\frac{\rho R_d}{\bar{\rho}h}\chi^2\,,\qquad(A8)$$

$$k_3=C\frac{\rho R_d}{\bar{\rho}h}\chi^3\,.\qquad(A9)$$

Here B and C are combinations of the disk radius R_d and half-thickness h defined in Eq. (7) and $\chi=(T_0/2\pi\rho R_d^2)^{1/2}$. Note also that here the meanings of the symbols x and y differ from their meanings in Sec. III B. With Θ and Δ as obtained by measurement, Eqs. (A1) and (A2) are solved simultaneously for u and w. The real and imaginary parts of the complex viscosity are then found from

$$\eta'=(u^2-w^2),\quad\eta''=-2uw\,.\qquad(A10)$$

Finally, η' and η'' are related to the viscosity η and elastic shear modulus G through Eq. (14). Our equations are a generalization to include end and edge effects of the working equations for an infinitely long oscillating-rod rheometer that have been presented by Oka [42].

As has been discussed above, in the case where the disk is surrounded by a Newtonian fluid, a consistency relation involving only the fluid density and instrumental constants holds between the period T and the damping Δ such that one may be calculated from the other. It is implicitly defined by eliminating of u between Eqs. (A1) and (A2) after w has been set to zero.

*Present address: Exxon Research and Engineering Co., Annandale, NJ 08801.

[1] For a review, see J. D. Gunton, M. San Miguel, and P. S. Sahni, in *Phase Transitions and Critical Phenomena*, edited by C. Domb and J. L. Lebowitz (Academic, New York, 1983), Vol. 8.

[2] J. S. Langer, M. Bar-On, and H. D. Miller, Phys. Rev. A **11**, 1417 (1975).

[3] J. S. Langer and A. J. Schwartz, Phys. Rev. A **21**, 948 (1980).

[4] E. D. Siggia, Phys. Rev. A **20**, 595 (1979).

[5] Y. C. Chou and W. I. Goldburg, Phys. Rev. A **20**, 2105 (1979).

[6] R. G. Howland, N. C. Wong, and C. M. Knobler, J. Chem. Phys. **73**, 522 (1980).

[7] N. C. Wong and C. M. Knobler, J. Chem. Phys. **69**, 725 (1978); Phys. Rev. A **24**, 3205 (1981).

[8] For example, see A. Onuki, K. Yamazaki, and K. Kawasaki, Ann. Phys. **131**, 217 (1981) for theory and D. Beysens, M. Gbadamassi, and B. Moncef-Bouanz, Phys. Rev. A **28**, 2491 (1983) for experiments.

[9] T. Imaeda, A. Onuki, and K. Kawasaki, Prog. Theor. Phys. **71**, 16 (1984); A. Onuki, Phys. Rev. A **34**, 3528 (1986).

[10] A. Onuki and S. Takesue, Phys. Lett. **114A**, 133 (1986); A. Onuki, Int. J. Thermophys. **10**, 293 (1989); Prog. Theor. Phys. Suppl. **99**, 382 (1990).

[11] F. Perrot, C. K. Chan, and D. Beysens, Europhys. Lett. **9**, 65 (1989); C. K. Chan, F. Perrot, and D. Beysens, Phys. Rev. A **43**, 1826 (1991); T. Baumberger, F. Perrot, and D. Beysens, Physica A **174**, 31 (1991).

[12] K. Y. Min, J. Stavans, R. Piazza, and W. I. Goldburg, Phys. Rev. Lett. **63**, 1070 (1989); N. Easwar, *ibid.* **68**, 186 (1992); K. Y. Min and W. I. Goldburg, *ibid.* **70**, 469 (1993).

[13] T. Baumberger, F. Perrot, and D. Beysens, Phys. Rev. A **46**, 7636 (1992).

[14] T. Takebe, K. Fujioka, R. Sawaoka, and T. Hashimoto, J. Chem. Phys. **93**, 5271 (1990) and references cited therein.

[15] K. Hamano, S. Yamashita, and J. V. Sengers, Phys. Rev. Lett. **68**, 3579 (1992).

[16] A. Onuki, Phys. Rev. A **35**, 5149 (1987).

[17] A. H. Krall, J. V. Sengers, and K. Hamano, Int. J. Thermophys. **10**, 309 (1989).

[18] A. H. Krall, J. V. Sengers, and K. Hamano, Phys. Rev. Lett. **69**, 1963 (1992).

[19] A. Emanuele and M. B. Palma-Vittorelli, Phys. Rev. Lett. **69**, 81 (1992).

[20] M. Doi and T. Ohta, J. Chem. Phys. **95**, 1242 (1991).

[21] J. Kestin, R. Paul, I. R. Shankland, and H.E. Khalifa, Ber. Bunsenges. Phys. Chem. **84**, 1255 (1980).

[22] A. H. Krall, J. V. Sengers, and J. Kestin, J. Chem. Eng. Data **37**, 349 (1992).

[23] S. C. Greer, T. E. Block, and C. M. Knobler, Phys. Rev. Lett. **34**, 250 (1975).

[24] A. Kumar, H. R. Krishnamurthy, and E. S. R. Gopal, Phys. Rep. **98**, 59 (1983).

[25] J. Kestin, I. R. Shankland, and R. Paul, Int. J. Thermophys. **5**, 3 (1984).

[26] C. K. Chan and W. I. Goldburg, Phys. Rev. Lett. **58**, 674 (1987).

[27] E. A. Clerke and J. V. Sengers, Physica A **118**, 360 (1983); A **120**, 367 (1983).

[28] R. F. Berg and M. R. Moldover, J. Chem. Phys. **89**, 3694 (1988).

[29] J. C. Nieuwoudt and J. V. Sengers, J. Chem. Phys. **90**, 457 (1989).

[30] H. Hao, Ph.D. Thesis, University of Maryland, College Park, 1991 (unpublished).

[31] D. Beysens, A. Bourgou, and P. Calmettes, Phys. Rev. A **26**, 3589 (1982).

[32] K. Hamano, S. Teshigawara, T. Koyama, and N. Kurahara, Phys. Rev. A **33**, 485 (1986).

[33] Y. Izumi and Y. Miyake, Phys. Rev. A **16**, 2120 (1977).

[34] K. Hamano (unpublished).

[35] S. C. Greer, Phys. Rev. A **14**, 1770 (1976).

[36] M. R. Moldover, Phys. Rev. A **31**, 1022 (1985).

[37] D. Woermann and W. Sarholz, Ber. Bunsenges. Phys. Chem. **69**, 319 (1965).

[38] Close to the critical point, non-Newtonian effects arise in the equilibrium mixtures because of critical slowing down. These effects are negligible for the values of the shear rate and frequency characteristic of our viscometer.

[39] G. F. Newell, J. Appl. Math. Phys. **10**, 160 (1959).

[40] J. C. Nieuwoudt, J. Kestin, and J. V. Sengers, Physica A **142**, 53 (1987).

[41] J. Kestin and I. R. Shankland, J. Non-Equilib. Thermodyn. **6**, 241 (1981).

[42] S. Oka, in *Rheology*, edited by F. R. Eirich (Academic, New York, 1960), Vol. 3.

[43] K. Kubota, N. Kuwahara, H. Eda, and M. Sakazume, Phys. Rev. A **45**, R37 (1992).

[44] W. H. Press, B. P. Flannery, S. A. Teukolsky, and W. T. Vetterling, *Numerical Recipes* (Cambridge University, New York, 1986).

[45] H. C. Burstyn, J. V. Sengers, and P. Esfandiari, Phys. Rev. A **22**, 282 (1980).

[46] The dependence of x, y, and z on the parameter c is readily shown to be of the form $x(\tau;f,\mu,c)=x(\tau;f,\mu,1)/c$ with similar equations holding for y and z.

[47] The numerical solutions indicate that $y(\tau)$ may be expressed as a combination of $\cos(\tau)$, $\sin(\tau)$, and harmonics with odd frequencies. Similarly, $x(\tau)$ may be expressed as a combination of a constant, $\cos(2\tau)$, $\sin(2\tau)$, and harmonics with even frequencies; the same is true of $z(\tau)$.

[48] G. I. Taylor, Proc. R. Soc. London, Ser. A **138**, 41 (1932).

[49] J. M. Rallinson, Ann. Rev. Fluid Mech. **16**, 45 (1984).

[50] J. G. Oldroyd, Proc. R. Soc. London, Ser. A **218**, 122 (1953).

[51] A. Cumming, P. Wiltzius, F. S. Bates, and J. H. Rosedale, Phys. Rev. A **45**, 885 (1992).

[52] A. Onuki (private communication).

[53] S. A. Khan and R. C. Armstrong, J. Rheol. **33**, 881 (1989).

[54] For conceptual simplicity here we write the consistency relation in this rough form.

[55] J. Bodensohn and W. I. Goldburg, Phys. Rev. A **46**, 5084 (1992).

[56] P. Guenoun, D. Beysens, and M. Robert, Phys. Rev. Lett. **65**, 2406 (1990).

[57] H. Princen, J. Colloid Interface Sci. **105**, 150 (1985).